



1

1 **Mechanistic representation of soil nitrogen emissions in the**
2 **Community Multi-scale Air Quality (CMAQ) model v 5.1**

3 **Quazi Z. Rasool^{1*}, Jesse O. Bash² and Daniel S. Cohan¹**

4 [1]{Department of Civil and Environmental Engineering, Rice University, Houston, Texas, USA}

5 [2]{Computational Exposure Division, National Exposure Research Laboratory, Office of Research and
6 Development, US Environmental Protection Agency, RTP, NC, USA}

7 *Currently at Department of Environmental Science and Engineering, UNC- Chapel Hill, NC, USA

8 *Correspondence to:* Quazi Rasool (qzr1@email.unc.edu)

1



9 **Abstract**

10 Soils are important sources of emissions of nitrogen (N)-containing gases such as nitric oxide
11 (NO), nitrous acid (HONO), nitrous oxide (N₂O), and ammonia (NH₃). However, most
12 contemporary air quality models lack a mechanistic representation of the biogeochemical
13 processes that form these gases. They typically use heavily parameterized equations to simulate
14 emissions of NO independently from NH₃, and do not quantify emissions of HONO or N₂O. This
15 study introduces a mechanistic, process-oriented representation of soil emissions of N species
16 (NO, HONO, N₂O, and NH₃) that we have recently implemented in the Community Multi-scale
17 Air Quality (CMAQ) model. The mechanistic scheme accounts for biogeochemical processes for
18 soil N transformations such as mineralization, volatilization, nitrification, and denitrification. The
19 rates of these processes are influenced by soil parameters, meteorology, land use, and mineral N
20 availability. We account for spatial heterogeneity in soil conditions and biome types by using a
21 global dataset for soil carbon (C) and N across terrestrial ecosystems to estimate daily mineral N
22 availability in non-agricultural soils, which was not accounted in earlier parameterizations for soil
23 NO. Our mechanistic scheme also uses daily year-specific fertilizer use estimates from the
24 Environmental Policy Integrated Climate (EPIC v.0509) agricultural model. A soil map with sub-
25 grid biome definitions was used to represent conditions over the continental United States. CMAQ
26 modeling for May and July 2011 shows improvement in model performance in simulated NO₂
27 columns compared to Ozone Monitoring Instrument (OMI) satellite retrievals for regions where
28 soils are the dominant source of NO emissions. We also assess how the new scheme affects model
29 performance for NO_x (NO+NO₂), fine nitrate (NO₃) particulate matter, and ozone observed by
30 various ground-based monitoring networks. Soil NO emissions in the new mechanistic scheme
31 tend to fall between the magnitudes of the previous parametric schemes and display much more
32 spatial heterogeneity. The new mechanistic scheme also accounts for soil HONO, which had been
33 ignored by parametric schemes.



34 **1 Introduction**

35 Global food production and fertilizer use are projected to double in this half-century in order to
36 meet the demand from growing populations (Frink et al., 1999; Tilman et al., 2001). Increasing
37 nitrogen (N) fertilization to meet food demand has been accompanied by increasing soil N
38 emissions across the globe, including in the United States (Davidson et al., 2011). N fertilizer
39 consumption globally has increased from 0.9 to 7.4 g N per m² cropland yr⁻¹ between 1961-2013,
40 with the U.S. still among the top five N fertilizer users in the world (Lu and Tian, 2017). U.S. N
41 fertilizer use increased from 0.28 to 9.54 g N m⁻² yr⁻¹ during 1940 to 2015. In the past century,
42 hotspots of N fertilizer use have shifted from the southeastern and eastern U.S. to the Midwest and
43 the Great Plains comprising the Corn Belt region (Cao et al., 2017). Recent studies have pointed
44 to soils as a significant source of NO_x emissions, contributing ~ 20% to the total budget globally
45 and larger fractions over heavily fertilized agricultural regions (Jaeglé et al., 2005; Vinken et al.,
46 2014; Wang et al., 2017). Soil NO emissions tend to peak in the summertime, when they can
47 contribute from 15-40% of total tropospheric NO₂ column in the continental U.S. (CONUS)
48 (Williams et al., 1992; Hudman et al., 2012; Rasool et al., 2016). Summer is also the peak season
49 for ozone concentrations (Cooper et al., 2014; Strode et al., 2015) and the time when
50 photochemistry is most sensitive to NO_x (Simon et al., 2014).

51 Despite the significance of NO_x emissions generated by soil microbes, policies both globally and
52 for CONUS have focused largely on limiting mobile and point fossil fuel sources of NO_x (Li et al.,
53 2016). Hence, it is incumbent to strategize for reduction of non-point soil sources of NO_x
54 emissions, especially in agricultural areas. Recent studies have shown higher soil NO_x even in non-
55 agricultural areas like forests to significantly impact summertime ozone in CONUS (Hickman et
56 al., 2010; Travis et al., 2016). Consequently, it is increasingly important to estimate both N
57 fertilizer-induced and non-agricultural NH₃ and NO_x emissions in air quality models.

58 N oxides (NO_x = NO + NO₂) worsen air quality and threaten human health directly and by
59 contributing to the formation of other pollutants. NO_x drives the formation of tropospheric ozone
60 and contributes to a significant fraction of both inorganic and organic particulate matter (PM)
61 (Seinfeld and Pandis, 2012; Wang et al., 2013). Global emissions of NO_x are responsible for one
62 in eight premature deaths worldwide as reported by the World Health Organization (Neira et al.,
63 2014). The premature deaths are a result of the link of these pollutants to cardiovascular and



4

64 chronically obstructive pulmonary (COPD) diseases, asthma, cancer, birth defects, and sudden
65 infant death syndrome. These adverse health impacts have been shown to worsen with the rising
66 rate of reactive N emissions from soil N cycling (Kampa and Castanas, 2008; Townsend et al.,
67 2003). NO_x indirectly impacts Earth's radiative balance by modulating concentrations of OH
68 radicals, the dominant oxidant of certain greenhouse gases such as methane (IPCC, 2007;
69 Steinkamp and Lawrence, 2011). Nitrous acid (HONO) upon photolysis releases OH radicals
70 along with NO, driving tropospheric ozone and secondary aerosol formation (Pusede et al., 2015).

71 Ammonia (NH_3) also contributes to a large fraction of airborne fine particulate matter ($\text{PM}_{2.5}$)
72 (Kwok et al., 2013). Elevated levels of $\text{PM}_{2.5}$ are linked to various adverse cardiovascular ailments
73 such as irregular heartbeat and aggravated asthma that cause premature death (Pope et al., 2009),
74 and contribute to visibility impairment through haze (Wang et al., 2012). NH_3 gaseous emissions
75 also influence the nucleation of new particles (Holmes, 2007). Air quality models such as,
76 Community Multiscale Air Quality (CMAQ) model and GEOS-Chem represent the bidirectional
77 NH_3 exchange between the atmosphere and soil-vegetation, analyzed under varied soil, vegetative,
78 and environmental conditions (Cooter et al., 2012; Bash et al., 2013; Zhu et al. 2015).

79 NO_x , NH_3 , HONO, and N_2O are produced from both microbial and physicochemical processes in
80 soil N cycling, predominantly nitrification and denitrification (Medinets et al., 2015; Parton et al.,
81 2001; Pilegaard, 2013; Su et al., 2011). Nitrification is oxidation of NH_4^+ to NO_3^- where
82 intermediate species such as NO and HONO are emitted along with relatively small amounts of
83 N_2O as byproducts. Denitrification is reduction of soil NO_3^- ; it produces some NO, but
84 predominantly produces N_2O and N_2 (Firestone and Davidson, 1989; Göttsche and Conrad, 2000;
85 Laville et al., 2011; Medinets et al., 2015). The fraction of N emitted as NO and HONO relative
86 to N_2O throughout nitrification and denitrification depends on several factors: soil temperature;
87 water filled pore space (WFPS), which in turn depends on soil texture and soil water content; gas
88 diffusivity; and soil pH. HONO is produced during nitrification only and is a source of NO and
89 OH after undergoing photolysis (Butterbach-Bahl et al., 2013; Conrad, 2002; Ludwig et al., 2001;
90 Oswald et al., 2013; Parton et al., 2001; Venterea and Rolston, 2000).

91 Whether N_2O or N_2 become dominant during denitrification depends on the availability of soil
92 NO_3^- relative to available carbon (C), WFPS, soil gas diffusivity, and bulk density (i.e., dry weight
93 of soil divided by its volume, indicating soil compaction/aeration by O_2). Denitrification rates are

4



5

94 quite low even at high soil N concentrations if available soil C is absent. However, the presence
95 of high NO_3^- concentrations with sufficient available C is the inhibiting factor for conversion of
96 N_2O to N_2 , keeping N_2O emissions dominant during denitrification (Weier et al., 1993; Del Grosso
97 et al., 2000). Denitrification N_2O emissions are also found to increase with a decrease in soil pH
98 in the range of 4.0 to 8.0 generally (Liu et al., 2010). Fertilizer application and wet and dry
99 deposition add to the soil NH_4^+ and NO_3^- pools, which undergo transformation to emit soil N as
100 intermediates of nitrification and denitrification (Kesik et al., 2006; Liu et al., 2006; Redding et
101 al., 2016; Schindlbacher et al., 2004).

102 Soil moisture content is the strongest determinant of nitrification and denitrification rates and the
103 relative proportions of various N gases emitted by each. Increasing soil water content due to
104 wetting events such as irrigation and rainfall can stimulate nitrification and denitrification.
105 Nitrification rates peak 2-3 days after wetting, when excess water has drained away and the rate
106 of downward water movement has decreased. Denitrification rates substantially increase and
107 nitrification rates become much slower in wetter soils. This is also influenced by soil texture; for
108 instance, denitrification is favored in poorly drained clay soils and nitrification is favored in freely
109 draining sandy soils (Barton et al., 1999; Parton et al., 2001).

110 WFPS is a metric that incorporates the above factors. Relative proportions of NO, HONO, and
111 N_2O emitted vary with WFPS. Dry aerobic conditions (WFPS ~ 0-55%) are optimal for
112 nitrification, with soil NO dominating soil N gas emissions at WFPS ~ 30–55% (Davidson and
113 Verchot, 2000; Parton et al., 2001). HONO emissions have been observed up to WFPS of 40%
114 and dominate N gas emissions under very dry and acidic soil conditions (Maljanen et al., 2013;
115 Mamtimin et al., 2016; Oswald et al., 2013; Su et al., 2011). Nitrification influences N_2O
116 production within the range of 30–70% WFPS, whereas denitrification dominates N_2O production
117 in wetter soils. Denitrification N_2O is limited by lower WFPS in spite of sufficient available NO_3^-
118 and C (Butterbach-Bahl et al., 2013; Del Grosso et al., 2000; Hu et al., 2015; Medinets et al., 2015;
119 Weier et al., 1993). As a result, NO and HONO emissions tend to decrease with increasing water
120 content, whereas N_2O emissions increase subject to available NO_3^- and C (Parton et al., 2001;
121 Oswald et al., 2013).

122 Extended dry periods also suppress soil NO emissions, by limiting substrate diffusion while water-
123 stressed nitrifying bacteria remain dormant, allowing N substrate (NH_4^+ or organic N) to

5



6

124 accumulate (Davidson, 1992; Jaeglé et al., 2004; Hudman et al., 2010; Scholes et al., 1997). Re-
125 wetting of soil by rain reactivates these microbes, enabling them to metabolize accumulated N
126 substrate (Homyak et al., 2016). The resulting NO pulses can be 10–100 times background
127 emission rates and typically last for 1–2 days (Yienger and Levy, 1995; Hudman et al., 2012;
128 Leitner et al., 2017).

129 Higher soil temperature is critical in increasing NO emission during nitrification under dry
130 conditions. However, N₂O generated in denitrification positively correlates with soil temperature
131 only when WFPS and N substrate availability in soil are not the limiting factors (Machefert et al.,
132 2002; Robertson and Groffman, 2007). Recently, a nearly 38% increase in NO emitted was
133 observed under dry conditions (~ 25–35 % WFPS) in California agricultural soils when soil
134 temperatures rose from 30–35 to 35–40 °C (Oikawa et al., 2015). Temperature-dependent soil NO_x
135 emissions may strongly contribute to the sensitivity of ozone to rising temperatures (Romer et al.,
136 2018). Also, some soil NO is converted to NO₂ and deposited to the plant canopy, reducing the
137 amount of NO_x entering the atmosphere (Ludwig et al., 2001).

138 Mechanistic models of soil N emissions already exist and are used in the earth science and soil
139 biogeochemical modeling community (Del Grosso et al., 2000; Manzoni and Porporato, 2009;
140 Parton et al., 2001). However, photochemical models like CMAQ have been using a mechanistic
141 approach only for NH₃, while using simpler parametric approaches for NO (Bash et al., 2013;
142 Rasool et al., 2016). Other N oxide emissions like HONO and N₂O are absent from the parametric
143 schemes used in CMAQ (Butterbach-Bahl et al., 2013; Heil et al., 2016; Su et al., 2011).
144 Variability in soil physicochemical properties like pH, temperature, and moisture along with
145 nutrient availability strongly control the spatial and temporal trends of soil N compounds
146 (Medinets et al., 2015; Pilegaard, 2013).

147 EPA's Air Pollutant Emissions Trends Data shows anthropogenic sources of NO_x fell by 60
148 percent in the U.S. since 1980, heightening the relative importance of soils. Area sources of NO_x
149 like soils along with less than expected reduction in off-road anthropogenic sources are believed
150 to have contributed to a slowdown in US NO_x reductions from 2011–2016 (Jiang et al., 2018).
151 Hence, accurate and consistent representation of soil N is needed to address uncertainties in their
152 estimates.

6



153 Parameterized schemes currently implemented in CMAQ for CONUS like Yienger-Levy (YL) and
154 the Berkeley Dalhousie Soil NO Parameterization (BDSNP) consider only NO expressed as a
155 fraction of total soil N available, without differentiating the fraction of soil N that occurs as organic
156 N, NH₄, or NO₃ (Hudman et al., 2012; Rasool et al., 2016; Yienger and Levy, 1995). Moreover,
157 these parametric schemes classify soil NO emissions as constant factors for different non-
158 agricultural biomes/ecosystems, compiled from reported literature and field estimates worldwide
159 (Davidson and Kinglerlee, 1997; Steinkamp and Lawrence, 2011; Yienger and Levy, 1995). These
160 emission factors account for the baseline biogenic NO_x emissions in addition to sources from
161 deposition (all biomes) and fertilizer (agricultural land-cover only) in the latest BDSNP
162 parameterization (Hudman et al., 2012; Rasool et al., 2016). Despite their limitations,
163 parameterized schemes do distinguish which biomes exhibit low NO emissions (wetlands, tundra,
164 and temperate or boreal forests) from those producing high soil NO (grasslands, tropical savannah
165 or woodland and agricultural fields) (Kottek et al., 2006; Rasool et al., 2016; Steinkamp and
166 Lawrence, 2011).

167 The U.S. Environmental Protection Agency (EPA) recently coupled CMAQ with U.S. Department
168 of Agriculture's (USDA) Environmental Policy Integrated Climate (EPIC) agro-ecosystem model.
169 This integrated EPIC-CMAQ framework accounts for a process-based approach for NH₃ by
170 modeling its bidirectional exchange (Nemitz et al., 2001; Cooter et al., 2010; Pleim et al., 2013).
171 The coupled model uses EPIC to simulate fertilizer application rate, timing, and composition.
172 Then, CMAQ estimates the spatial and temporal trends of the soil ammonium (NH₄⁺) pool by
173 tracking the ammonium mass balance throughout processes like fertilization, volatilization,
174 deposition, and nitrification (Bash et al., 2013). Using the EPIC-derived soil N pool better
175 represents the seasonal dynamics of fertilizer-induced N emissions across CONUS (Cooter et al.,
176 2012). The coupling with EPIC reduces CMAQ's error and bias in simulating total NH₃ + NH₄⁺
177 wet deposition flux and ammonium related aerosol concentrations (Bash et al., 2013). BDSNP
178 parametric scheme implemented in CMAQ also uses the daily soil N pool from EPIC (Rasool et
179 al., 2016).

180 Our work builds a new mechanistic approach for modeling soil N emissions in CMAQ based on
181 DayCENT (Daily version of CENTURY model) biogeochemical scheme (Del Grosso et al., 2001;
182 Parton et al., 2001), integrating nitrification and denitrification mechanistic processes that generate



183 NO, HONO, N₂O, and N₂ under different soil conditions and meteorology. We compare the NO
184 and HONO emissions estimates and associated estimates of tropospheric NO₂ column, ozone, and
185 PM_{2.5} with those obtained from CMAQ using the YL and BDSNP parametric schemes. For
186 agricultural biomes, our mechanistic scheme uses daily soil N pools from the same EPIC
187 simulations as in Rasool et al. (2016). Unlike BDSNP, which uses a total weighted soil N, the new
188 mechanistic model tracks different forms of soil N as NH₄, NO₃, and organic N for different soil
189 layers and vegetation types so that, nitrification and denitrification can be represented. For non-
190 agricultural biomes, our new mechanistic scheme uses a global soil nutrient dataset in an updated
191 C and N mineralization framework. This enables the model to track the conversion of organic soil
192 N to NH₄ and NO₃ pools on a daily scale for non-agricultural soils.

193

194

195 **2 Methodology**

196

197 **2.1 Overview of soil N schemes**

198

199 Key features of the YL and BDSNP parametric soil NO schemes and our new mechanistic scheme
200 for soil NO, HONO, and N₂O are illustrated in Figure 1 and Table 1.

201 The YL scheme, based on Yienger and Levy (1995), parameterizes soil NO emission
202 ($S_{NO_{YL}}$, in $ng - N m^{-2} s^{-1}$) in Equation 1 as a function of biome specific emissions factor
203 (A_{biome}) and soil temperature (T_{soil}).

$$204 \quad S_{NO_{YL}} = f_{\frac{w}{d}} \left(A_{biome(w/d)}, T_{soil} \right) P(\text{precipitation}) CRF(LAI, SAI) \quad (1)$$

205 The emissions factor depends on whether the soil is wet ($A_{biome(w)}$) or dry ($A_{biome(d)}$), with the
206 wet factor used when rainfall exceeds one cm in the prior two weeks. For dry soils, YL assumes
207 NO emissions exhibit a small and linear response to increasing soil temperatures. For wet soils,
208 soil NO is zero for frozen conditions, increases linearly from 0 to 10°C, and increases
209 exponentially from 10 to 30°C, after which it is constant. In agricultural regions, YL assumes wet



9

210 conditions throughout the growing season (May – September) and assumes 2.5% of the fertilizer
 211 applied N is emitted as NO, in addition to a baseline NO emissions rate based on grasslands. The
 212 pulsing term ($P(\textit{precipitation})$) is applied if precipitation follows at least two dry weeks. The
 213 canopy reduction factor (CRF) is set as a function of leaf area index (LAI) and stomatal area index
 214 (SAI).

215 Biogenic Emissions Inventory System (BEIS v.3.61 used in current versions of CMAQ (v5.0.2 or
 216 higher) estimates NO emissions from soils essentially using the same original YL algorithm as in
 217 Equation 1, with slight updates accounting for soil moisture, crop canopy coverage, and fertilizer
 218 application. The YL soil NO algorithm in CMAQ distinguishes between agricultural and
 219 nonagricultural land use types (Pouliot and Pierce, 2009). Adjustments due to temperature,
 220 precipitation (pulsing), fertilizer application, and canopy uptake are limited to the growing season,
 221 assumed as April 1 to October 31, and are restricted to agricultural areas as defined by the Biogenic
 222 Emissions Landuse Database (BELD). Unlike the original YL, the implementation of YL in
 223 CMAQ (CMAQ-YL) interpolates between wet and dry conditions based on soil moisture in the
 224 top layer (1cm). In this study, we use the Pleim-Xiu Land Surface Model (PX-LSM) in CMAQ to
 225 compute soil temperature (T_{soil}) and soil moisture (θ_{soil}).

226 Agricultural soil NO emissions are based on the baseline grassland NO emission ($A_{grassland}$) plus
 227 an additional factor ($Fertilizer(t)$) that starts at its peak value during the first month of the
 228 growing season and declines linearly to zero at the end of the growing season. The growing season
 229 is defined as April-October in CMAQ-YL, rather than being allowed to vary by latitude (original
 230 YL) or by a satellite driven analysis of vegetation (original BDSNP). A summary of the modified
 231 YL algorithm is presented below for growing season agricultural emissions (Equation 2).

232 $S_{NO_{CMAQ-YL, Agricultural\ growing\ season}} =$

233 $f(A_{grassland} + Fertilizer(t), T_{soil}, \theta_{soil})P(\textit{precipitation})CRF(LAI, SAI) \quad (2)$

234 For non-growing season or non-agricultural areas throughout the year, soil NO emissions are
 235 assumed to depend only on temperature and the base emissions for different biomes (A_{biome}) as
 236 provided in BEIS. CMAQ still uses the base emission for both agricultural and non-agricultural

9



237 land types with adjustments based solely on air temperature ($T_{air,in K}$) as done in BEIS (Equation
238 3).

$$239 \quad S_{NO_{CMAQ-YL}, \text{ non-agricultural or non-growing season}} \\ 240 \quad = (A_{biome})e^{(0.04686 * T_{air} - 14.30579)} \quad (3)$$

241 The original implementation of the BDSNP scheme in CMAQ v5.0.2 was described by Rasool et
242 al. (2016). Here, we update that code for CMAQv5.1, but the formulation remains the same. Soil
243 NO emissions, S_{NO} , are computed in Equation 4 as the product of biome specific emission rates
244 ($A_{biome}(N_{avail})$) and adjustment factors to represent the influence of ambient conditions. The
245 biome specific emission rates have background soil NO for 24 MODIS biome types from literature
246 (Stehfest and Bouwman, 2006; Steinkamp and Lawrence, 2011). Fertilizer and deposition
247 emission rates based on an exponential decay after input of fertilizer and deposition N are added
248 to background soil NO emission rates for respective biomes. BDSNP accounts for total N from
249 fertilizer and deposition obtained from EPIC. EPIC provides the N available from crop-specific
250 fertilizer soil N pool in different forms as: NH_4 , NO_3 , and organic N. A final weighted total soil N
251 pool is used by weighting the different N forms by the fraction of each crop type in each modeling
252 grid. The soil temperature response $f(T_{soil})$ is an exponential function of temperature (in K). Unlike
253 YL that depends solely on rainfall, BDSNP has a Poisson function $g(\theta)$ based on soil moisture
254 (θ) that increases smoothly first until a maximum and then decreases when soil becomes water-
255 saturated. BDSNP also differentiates between wet and dry soil conditions and provides more
256 detailed representation than YL of pulsing following precipitation and of the CRF (described in
257 section 2.5).

$$258 \quad S_{NO_{BDSNP}} = A_{biome}(N_{avail}) f(T)g(\theta)P(l_{dry})CRF(LAI, Meteorology, Biome) \quad (4)$$

259 Our new mechanistic scheme computes soil emissions of NO, HONO, and N_2O by specifically
260 representing both nitrification and denitrification. Equations 5-7 provide an overview of the
261 mechanistic formulation. All functions are described in greater detail in Section 2.6.4. In the
262 equations, the pulsing factor $P(l_{dry})$ follows the formulation of Rasool et al. (2016). The canopy
263 reduction factor $CRF(LAI, Meteorology, Biome)$ is described in section 2.5. Briefly, we note
264 that nitrification rates (R_N in Eq. 24, $kg - N/ha \text{ per s}$) depend on the available NH_4 pool, soil



265 temperature (T_{soil}), soil moisture (θ_{soil}), gas diffusivity (Dr), and pH adjustment factors.
 266 Meanwhile, denitrification rates (R_D in Eq. 25, $kg - N/ha$ per s) depend on available NO_3
 267 pool, relative availability of NO_3 to C, soil temperature, gas diffusivity, and soil moisture
 268 adjustment factors.

$$\begin{aligned}
 269 \quad S_{NO} &= \left(\begin{array}{c} N_{NO_x} - S_{HONO} \\ + \\ D_{NO} \end{array} \right) CRF(LAI, Meteorology, Biome) \\
 270 \quad &\equiv \left(\begin{array}{c} f(NH_4, T_{soil}, \theta_{soil}, Dr, pH)P(l_{dry}) \\ + \\ f(NO_3: C, T_{soil}, \theta_{soil}, Dr) \end{array} \right) CRF(LAI, Meteorology, Biome) \quad (5)
 \end{aligned}$$

$$\begin{aligned}
 271 \quad S_{HONO} &= (HONO_f)(N_{NO_x})(f_{SWC})CRF(LAI, Meteorology, Biome) \\
 272 \quad &\equiv (HONO_f) \left(f(NH_4, T_{soil}, \theta_{soil}, Dr, pH)P(l_{dry}) \right) (f_{SWC})CRF(LAI, Meteorology, Biome) \quad (6)
 \end{aligned}$$

$$273 \quad S_{N_2O} = \left(\begin{array}{c} N_{N_2O} \\ + \\ D_{N_2O} \end{array} \right) \equiv \left(\begin{array}{c} f(NH_4, T_{soil}, \theta_{soil}, Dr, pH) \\ + \\ f(NO_3: C, T_{soil}, \theta_{soil}, Dr) \end{array} \right) \quad (7)$$

274 In all our simulations, soil NH_3 emission is calculated based on the bi-directional exchange scheme
 275 (Bash et al., 2013) in CMAQ.

276

277 **2.2 Biome classification over CONUS**

278 CMAQ uses the National Land Cover Database with 40 classifications (NLCD40,
 279 <https://www.mrlc.gov/>) to represent land cover, which is used by the YL parametric scheme.
 280 However, Steinkamp and Lawrence (2011) provide soil NO emission factors ($A'_{biome}(N_{avail})$)
 281 for only 24 MODIS biomes in the BDSNP parametric scheme. Thus, the initial implementation of
 282 BDSNP in CMAQ by Rasool et al. (2016) introduced a mapping between MODIS 24 and NLCD40
 283 biomes to set an emission factor for each NLCD40 biome type (see Appendix Table A2). Factors
 284 were then adjusted using Köppen climate zone classifications (Kottek et al., 2006). Whereas the
 285 original implementation of BDSNP by Rasool et al. (2016) treated each grid cell based on its most
 286 prevalent biome type, our update of BDSNP for CMAQv5.1 and our mechanistic model use sub-
 287 grid biome classification, accounting for the fraction of each biome type in each cell.



288 The latest Biogenic Emissions Landcover Database version 4 (BELD4), generated using the
289 BELD4 tool in the SA Raster Tools system, is used to represent land cover types consistently
290 across both the Fertilizer Emission Scenario Tool for CMAQ (FEST-C v1.2,
291 <https://www.cmascenter.org/fest-c/>); and the Weather Research and Forecast (WRF)
292 meteorological model (Skamarock et al., 2008)/CMAQ framework. BEIS v3.61 within CMAQ
293 integrates BELD4 with other data sources generated at 1-km resolution to provide fractional crop
294 and vegetation cover. U.S. land use categories are based on the 2011 NLCD40 categories. FEST-
295 C provides tree and crop percentage coverage for 194 tree classes and 42 crops
296 (https://www.cmascenter.org/sa-tools/documentation/4.2/Raster_Users_Guide_4_2.pdf). For
297 determining fractional crop cover, the 2011 NLCD/MODIS data was used for Canada and the U.S.
298 in BELD4 data generation tool of FEST-C. Tree species fractional coverage is based on 2011
299 Forest Inventory and Analysis (FIA) version 5.1. MODIS satellite products are used where detailed
300 data is unavailable outside of the U.S.

301

302 **2.3 N Fertilizer**

303 The YL scheme set fertilizer-driven soil NO emissions to be proportional to fertilizer application
304 during a prescribed growing season: May-August for the Northern Hemisphere and November-
305 February for the Southern Hemisphere (Yienger and Levy, 1995) or April-October for CMAQ-
306 YL. Our implementations of both BDSNP parameterization and mechanistic soil N schemes into
307 CMAQ are designed to enable the use of year- and location-specific fertilizer data with daily
308 resolution. We use FEST-C to incorporate EPIC fertilizer application data into our CMAQ runs.
309 EPIC estimates daily fertilizer application based entirely on simulated idealized plant demand with
310 N stress and limitations in response to local soil and weather conditions, using linkages with WRF
311 via FEST-C. The FEST-C interface also ensures EPIC simulations are spatially consistent with
312 CMAQ's CONUS domain and resolution through the Spatial Allocator (SA) Raster Tools system
313 (<http://www.cmascenter.org/sa-tools/>).

314 Because EPIC covers only the U.S., outside the U.S. BDSNP use fertilizer data regridded from
315 Hudman et al. (2012), which scaled Potter et al. (2010) data for fertilizer N from 1994-2001 to



316 global fertilizer levels in 2006. Our mechanistic scheme uses a more recently compiled and
317 speciated soil N and C dataset for non-U.S. agricultural regions, regridded from Xu et al. (2015).

318

319 **2.4 N Deposition**

320 N deposition serves as a significant addition to the soil mineral N (inorganic N: NH_4^+ and NO_3^-)
321 pool and hence influences soil N emissions. The YL scheme does not explicitly represent N
322 deposition but instead sets soil emissions based on biome type. In our implementation of both
323 updated BDSNP and new mechanistic soil N schemes, hourly wet and dry deposition rates for both
324 reduced and oxidized forms of N, computed within the CMAQ simulation, are added to the NH_4^+
325 and NO_3^- soil pools.

326

327 **2.5 Canopy reduction factor (CRF)**

328 CRF is used to calculate above canopy NO and HONO, assuming that some fraction of each is
329 converted to NO_2 and absorbed by leaves. Earlier global scale GEOS-Chem simulations with
330 BDSNP had a monthly averaged CRF that reduced total soil NO_x by an average of 16% (Hudman
331 et al., 2012).

332 The original YL soil NO scheme (Yienger and Levy, 1995) and the in-line BEIS in CMAQ set
333 CRF as a function of LAI and SAI. Recently, implementations of BDSNP in CMAQ and GEOS-
334 Chem implemented CRF as a function of wind speed, turbulence, and canopy structure (Geddes et
335 al., 2016; Rasool et al., 2016; Wang et al., 1998).

336 Here, we compute CRF using equations from Wang et al. (1998) for both BDSNP and the new
337 mechanistic scheme using spatially and temporally variable land-surface parameters: surface (2
338 m) temperature, solar radiation (W/m^2), surface pressure, snow cover, wind speed (v_{wind}), cloud
339 fraction, canopy structure, vegetation coverage (LAI and canopy resistances), gas diffusivity, and
340 deposition coefficients. The final reduction factor ($CRF(\text{LAI}, \text{Meteorology}, \text{Biome})$) for primary
341 biogenic soil NO emissions is based on two main factors: bulk stomatal resistance (R_{Bulk}), and



342 land-use specific ventilation velocity of NO ($v_{vent,NO}$), calculated based on the parameters
 343 mentioned above (Equation 8).

$$344 \quad CRF(LAI, Meteorology, Biome) = \frac{R_{Bulk}}{R_{Bulk} + v_{vent,NO}} \quad (8)$$

345 Ventilation velocity of NO ($v_{vent,NO}$) is calculated by adjusting a normalized day and night
 346 specific velocity from Wang et al.: 10^{-2} and 0.2×10^{-2} m/s, respectively. The adjustments are based
 347 on biome-specific LAI and canopy wind extinction coefficients (C_{Biome}). $C_{tropical\ rainforest}$ is the
 348 canopy wind extinction coefficient for tropical rain forests, the biome on which most canopy
 349 uptake studies for NO_x are based (Equation 9).

$$350 \quad v_{vent,NO} = v_{vent,NO\ day/night} \sqrt{\left(\frac{v_{wind}}{3}\right)^2 \left(\frac{7}{LAI}\right) \left(\frac{C_{tropical\ rainforest}}{C_{Biome}}\right)} \quad (9)$$

351 R_{Bulk} is a combination of various canopy resistances in series and parallel: internal stomatal
 352 resistance, cuticle resistance, and aerodynamic resistance which have biome specific normalized
 353 values for the MODIS 24 biomes also available in the dry deposition scheme of CMAQ. These
 354 normalized values of individual resistances are subsequently adjusted and dependent on multiple
 355 conditions for solar radiation, surface temperature, pressure, deposition coefficients and molecular
 356 diffusivity of NO₂ in air. The calculation of R_{Bulk} based on Wang et al. (1998) has been
 357 documented and shared in the open source BDSNP code repository (canopy_nox_mod.F) for the
 358 purpose of reproducibility, available at https://daac.ornl.gov/cgi-bin/dsviewer.pl?ds_id=1351.

359

360 **2.6 Detailed description of the mechanistic soil N scheme**

361 **2.6.1 Overview**

362 Our new mechanistic soil N model tracks the NH₄, NO₃, and organic C and N pools in soil
 363 separately, in contrast to the total N pool of BDSNP, and estimates NO, HONO, and N₂O rather
 364 than just NO (Figure 2). It uses DayCENT to represent both nitrification and denitrification. For
 365 agricultural biomes, we use speciated N and C pools from EPIC to drive DayCENT. For non-



366 agricultural biomes, we use a C-N mineralization framework (Manzoni and Porporato, 2009) to
367 estimate the inorganic N and C pools for DayCENT.

368 One of the advantages of using DayCENT is its ability to simulate all types of terrestrial
369 ecosystems. DayCENT is one of the only biogeochemical models which not only provides a
370 process-based representation of soil N emissions, but has also been calibrated and validated across
371 an array of conditions for crop productivity, soil C, soil temperature and water content, N₂O, and
372 soil NO₃⁻ (Necpálová et al., 2015). Hence, mechanistic models like DayCENT yield more reliable
373 results by applying validated controls of soil properties like soil temperature and moisture, which
374 are the key process controls to nitrification and denitrification. More recent mechanistic models
375 like DNDC, MicNit, ECOSYS, and COUPMODEL are quite similar to DayCENT in the
376 representation of nitrification and denitrification process. However, these models have not been as
377 widely evaluated and impose greater computational costs (Butterbach-Bahl et al., 2013).
378 DayCENT also enhances consistency in our mechanistic model by utilizing the same C-N
379 mineralization scheme (taken from the CENTURY model (Parton et al., 2001)) that is used in
380 EPIC.

381 Most stand-alone applications of DayCENT and other mechanistic models have focused on the
382 biogeochemical, climate, and agricultural impacts of soil emissions. Our linkage of DayCENT
383 with CMAQ provides an opportunity to for the first time estimate emissions of multiple soil N
384 species through a process-based approach and then assess their impact on atmospheric chemistry
385 in a regional photochemical model.

386 **2.6.2 Agricultural regions**

387 In agricultural regions, we use EPIC to derive organic N, NH₄, NO₃, and C pools updated on a
388 daily scale. EPIC follows the same approach used in the CENTURY model (Parton et al., 1994),
389 but uses an updated crop growth model, and better represents effect of sorption on soil water
390 content that affect leaching losses and surface to sub-surface flow of N. In contrast, CENTURY
391 used monthly water leached below 30-cm soil depth, annual precipitation, and the silt and clay
392 content of soil (Izaurre et al., 2006).

393 In EPIC, organic N residues added to the agricultural soil surface or belowground from plant/crop
394 residues, roots, fertilizer, deposition and manure are split into two broad compartments: microbial



395 or active biomass, and slow or passive humus. Slow or passive humus is essentially recalcitrant
396 and non-living in nature with very slow turnover rates ranging from centuries to even thousands
397 of years and makes up most of the organic matter. N uptake by soil microbes from organic matter,
398 also called ‘microbial biomass’ or ‘microbial/active N,’ is the living portion of the soil organic
399 matter, excluding plant roots and soil animals larger than $5 \times 10^{-3} \mu\text{m}^3$. Although, microbial
400 biomass constitutes a small portion of organic matter (~ 2%), it is central in microbial activity, in
401 other words conversion of organic N to inorganic N (Cameron and Moir, 2013; Manzoni and
402 Porporato, 2009). The transformation rate of organic N to microbial N is controlled by the relative
403 C and N content in microbial biomass, soil temperature and water content, soil silt and clay content,
404 organic residue composition- enhanced by tillage in agricultural soil, bulk density, oxygen content,
405 and inorganic N availability. Microbial N has quicker turnover times ranging from days to weeks
406 compared to hundreds of years for slow or passive organic matter (Izaurralde et al., 2006; Schimel
407 and Weintraub, 2003). Hence, microbial biomass is the main clearinghouse and driver of C and N
408 cycling in EPIC. Whether net mineralization of organic N to NH_4^+ occurs or net immobilization
409 of NO_3^- to microbial N depends strongly on the relative C and N contents in microbial biomass.
410 Higher N content supports net mineralization, whereas higher C content supports net
411 immobilization. C and N can also be leached or lost in gaseous forms (Izaurralde et al., 2012).

412 We then estimate gaseous N emissions by using the organic N, NH_4 , NO_3 , and C pools provided
413 from EPIC/FEST-C along with relevant soil properties for agricultural biomes from the DayCENT
414 nitrification and denitrification sub-model, as described in Section 2.6.4 and illustrated in Figure
415 2.

416 **2.6.3 Non-agricultural regions**

417 We adapt the framework for linked C and N cycling from Schimel and Weintraub (2003) for non-
418 agricultural regions, where EPIC is not applicable. This framework accounts for the mineralization
419 of organic N by considering which element is limiting based on relative C to N content in microbial
420 biomass. If N is in excess, then mineralization of organic N producing NH_4^+ is favored. If C is in
421 excess, it results in overflow metabolism that results in elevated C respiration rates that are not
422 associated with microbial growth. The resultant inorganic N and C respiration rates are then
423 applied on a temporal and spatial scale consistent with those for the EPIC agricultural pool.



424 To ensure mass balance, enzyme production (Equations 11-13) and recycling mechanisms
 425 (Equations 14-15) to replenish microbial biomass C are crucial. Similarly, net immobilization is
 426 assumed as was done in EPIC, when we approach C saturated conditions with time to replenish
 427 microbial N. Without such mechanisms, there is a danger to always incorrectly predict N or C-
 428 limited state for microbes. Also, some proportion of the microbial biomass is utilized for
 429 maintenance of living cells (only C demand) (Equation 14), while the rest accounts for decay and
 430 regrowth (both C and N demands) (Equations 16-17, 18-19) (Schimel and Weintraub, 2003;
 431 Manzoni and Porporato, 2009). Fractions of C and N in dying microbial biomass are recycled into
 432 the available microbial C and N pools. Schimel and Weintraub (2003) provide values for
 433 parameters that quantify these growth and decay processes: Fraction of Biome C to exoenzymes
 434 (K_e) = 0.05; microbial maintenance rate (K_m) = 0.01 d⁻¹; substrate use efficiency (SUE) = 0.5;
 435 Proportion of microbial biomass that dies per day (K_t) = 0.012 d⁻¹; Proportion of microbial biomass
 436 (C or N) for microbial use (K_r) = 0.85.

$$437 \quad R_m \text{ (Respiration from maintenance)} = K_m(SMC) \quad (10)$$

$$438 \quad R_e \text{ (Respiration from enzyme production)} = ((1 - SUE)(EP_C)/SUE) \quad (11)$$

$$439 \quad EP_C \text{ (Enzyme production as C Loss/Sink)} = K_e(SMC) \quad (12)$$

$$440 \quad EP_N \text{ (Enzyme production as N Loss/Sink)} =$$

$$441 \quad EP_C/3 \text{ (Where 3 is the approximate C:N ratio for protien)} \quad (13)$$

$$442 \quad CY_C \text{ (Recycle from C microbial biomass)} = K_t K_r(SMC) \quad (14)$$

$$443 \quad CY_N \text{ (Recycle from N microbial biomass)} = CY_C/C_m : N_m \quad (15)$$

$$444 \quad H_C \text{ (C Death/decay)} = K_t(1 - K_r)(SMC) \quad (16)$$

$$445 \quad H_N \text{ (N Death/decay)} = H_C/C_m : N_m \quad (17)$$

446 *If C limited or N in excess:*

$$447 \quad SMC < R_m + (EP_C/SUE) + ((SMN - EP_N)(C_m : N_m/SUE)) \quad (18)$$

$$448 \quad R_g \text{ (Respiration from growth, C limited)} = (1 - SUE)(SMC - (EP_C/SUE) -$$

$$449 \quad R_m) \quad (19)$$



450 R_O (Respiration from overflow mechanism) = 0 (20)

451 NH_4 (From net mineralization after mass balance) = $(SMN - EP_N - ((SMC -$
452 $(EP_C/SUE) - R_m)(SUE/C_m: N_m)))$ (21)

453 We represent spatial heterogeneity in soil C and N by using the Schimel and Weintraub (2003)
454 algorithm with sub-grid land use fractions from NLCD40 to estimate the different parameters for
455 specific non-agricultural biomes in Equations 10-20. That allows us to account for inter-biome
456 variability in soil properties and organic/microbial biomass.

457 Mineralized N pools generated as NH_4 in this framework are calculated eventually as a function
458 of microbial biomass and aforementioned parameters driving the net mineralization (Equations 18
459 and 21).

460 We map a global organic C and N pool dataset (Xu et al., 2015) onto our CONUS domain, using
461 biome-specific fractions from 12 different biome types for conversion of these organic pools into
462 microbial biomass pools (Xu et al., 2013). We map these 12 broader biome types to the 24 MODIS
463 biome types by the mapping shown in Table A1. To ensure consistency with the sub-grid biome
464 fractions for the 40 NLCD biome types (section 2.2), we map the MODIS 24 biome-specific
465 microbial/Organic C and N fractions to NLCD 40 ($C_{mic_{biome}}$ and $N_{mic_{biome}}$, $biome$ represents
466 the 40 NLCD categories) by the mappings shown in Tables A2 and A3. We calculate area-
467 weighted microbial C and N pools (SMC and SMN) using $C_{mic_{biome}}$ and $N_{mic_{biome}}$ that account
468 for the inter-biome variability in availability of soil microbial biomass. Also, spatial heterogeneity
469 in terms of vertical stratification is crucial as emission losses from N cycling primarily happen in
470 the top 30-cm layer. Hence we incorporate the Xu et al. (2015) data for the top 30 cm for organic
471 nutrient pool and microbial C:N ratio ($C_m: N_m$) along with other soil properties such as soil pH,
472 θ_{soil} , and T_{soil} . This framework (Figure 2) enables us to estimate soil NH_4 , NO_3 , and C pools from
473 area-weighted microbial biomass as consistently as possible with the pools that EPIC provides in
474 agricultural regions.

475 **2.6.4 DayCENT representation of soil N emissions**

476 The final part of the mechanistic framework is formed by using a nitrification and denitrification
477 N emissions sub-model adapted from DayCENT along with nitrification and denitrification rate
478 calculations adapted from EPIC. Nitrification and denitrification rates are adapted from EPIC to



479 maintain consistency with NH₃ bi-directional scheme in CMAQ, which uses the same. It should
 480 be noted that the coupled C–N decomposition module in the EPIC terrestrial ecosystem model is
 481 similar to that of DayCENT (Izaurre et al., 2012; Gaillard et al., 2017). EPIC simulated
 482 agricultural NH₄ and NO₃ soil pools are generated as described in Section 2.6.2, whereas the non-
 483 agricultural NH₄ and NO₃ soil pools are calculated by the methods described in Section 2.6.3
 484 (Equations 22-23). NH₄ and NO₃ soil pools drive nitrification and denitrification as shown in
 485 Equations 24-25. Variability in terms of soil conditions influencing N emissions in nitrification
 486 and denitrification are introduced through the rates at which NH₄ is nitrified (R_N) and NO₃ is
 487 denitrified (R_D) (Equations 24-25).

488 The nitrification rate (K_N) (Equation 26) is estimated based on regulators from the soil water
 489 content, soil pH, and soil temperature (T_{soil}), following the approach of Williams et al. (2008),
 490 consistent with the bi-directional NH₃ scheme in CMAQ (Bash et al., 2013). The nitrification soil
 491 temperature regulator (f_T) accounts for frozen soil with no evasive N fluxes (Equation 27). The
 492 nitrification soil water content regulator (f_{SW}) accounts for soil water content at wilting point and
 493 field capacity (Equations 28-29). The regulator terms f_T and f_{SW} both get their dependent
 494 variables from Meteorology-Chemistry Interface Processor (MCIP) (Otte and Pleim, 2010)
 495 derived land-surface outputs. However the nitrification soil pH regulator (f_{pH}) takes soil pH for
 496 agriculture soil from EPIC and for non-agricultural soil from a separate global dataset (Xu et al.,
 497 2015), available at both 0.01 m and 1 m depths to maintain consistency with MCIP (Equation 30).
 498 Denitrification rate (K_D) (Equation 31) is regulated by soil temperature (Equation 34), with WFPS
 499 (Equation 33) acting as a proxy for O₂ availability and soil moisture (θ_{soil}), and relative
 500 availability of NO₃ and C (Equation 32) determining N₂O or N₂ emissions during denitrification
 501 (Williams et al., 2008). Note that Equations 26 and 31 set upper limits for K_N and K_D , respectively.

$$502 \quad NO_3(kg - N/ha, after Nitrification) = NH_4 (1.0 - e^{-(K_N dt)}) \quad (22)$$

$$503 \quad NH_4(kg - N/ha, after Nitrification) = NH_4 e^{-(K_N dt)} \quad (23)$$

$$504 \quad R_N(kg - N/ha per s) = NH_4 (1.0 - e^{-(K_N dt)})/dt \quad (24)$$

$$505 \quad R_D(kg - N/ha per s) = NO_3 (1.0 - e^{-(K_D dt)})/dt \quad (25)$$

$$506 \quad K_N(s^{-1}) = \min(0.69, (f_T)(f_{SW})(f_{pH})) \quad (26)$$



507 f_T (Nitrification soil temperature regulator) = $\max(0.041(T_{soil} - 278.15), 0.0)$ (27)

508 f_{SW} (Nitrification soil water content regulator)

509 =
$$\begin{cases} 0.1, & \text{If } (\theta_{soil} \leq \text{wilting point}) \\ \max\left(0.1, 0.1 + 0.9 \sqrt{\frac{(\theta_{soil} - \text{wilting point})}{(\text{field capacity} - \text{wilting point})}} \cdot \frac{(\theta_{soil} - \text{wilting point})}{0.25(\text{field capacity} - \text{wilting point})}\right), & \text{If } (wg25 > \theta_{soil} > \text{wilting point}) \\ 1.0, & \text{If } (\text{field capacity} > \theta_{soil} \geq wg25) \\ \max\left(0.1, 1.0 - \frac{(\theta_{soil} - \text{field capacity})}{(\theta_{soil}(\text{at Saturation}) - \text{field capacity})}\right), & \text{If } (\theta_{soil} > \text{field capacity}) \end{cases}$$
 (28)

510 $wg25 = \text{wilting point} + 0.25(\text{field capacity} - \text{wilting point})$ (29)

511 f_{pH} (Nitrification soil pH regulator)

512 =
$$\begin{cases} 0.307(pH) - 1.269, & \text{Acidic soil } (pH < 7) \\ 1.0, & \text{Neutral soil } (7.4 > pH \geq 7) \\ 5.367 - 0.599(pH), & \text{Alkaline soil } (pH \geq 7.4) \end{cases}$$
 (30)

513 $K_D (s^{-1}) = \min(0.01, f(WFPS, T_{soil}, NO_3 : C))$ (31)

514 $f(WFPS, T_{soil}, NO_3 : C)$, Denitrification regulators

515 =
$$(f_{T,D}) (f_{WFPS,D}) \left(\frac{(1.4(LabileC)(NO_3))}{((LabileC + 17)(NO_3 + 83))} \right)$$
 (32)

516 $f_{WFPS,D} = \min\left(1.0, \frac{4.82}{14(16/(12(1.39(WFPS))))}\right)$ (33)

517 $f_{T,D} = \min\left(1.0, e^{\left(308.56\left(\frac{1}{68.02} - \frac{1}{T_{soil}(\text{in K}) - 227.13}\right)\right)}\right)$ (34)

518 DayCENT partitions N emissions as NO_x and N_2O based on relative gas diffusivity in soil
 519 compared to air (Dr) (Equation 35). Dr is calculated based on the algorithm from Moldrup et al.
 520 (2004), which accounts for soil water content, soil air porosity, and soil type. Also, Dr and hence
 521 the ratio of NO_x to N_2O emissions (r_{NO_x/N_2O}) being a function of Dr , accounts for soil texture by
 522 quantifying pore space, which is highest in coarse soil (Parton et al., 2001; Moldrup et al., 2004).
 523 DayCENT assumes 2% of nitrified N (R_N) is lost as N_2O (Equation 36). r_{NO_x/N_2O} is the ratio of



524 NO_x (both NO and HONO, which photolyses rapidly to NO) to N_2O , where emissions are
 525 expressed on g-N/hr basis. These emissions are susceptible to pulsing after re-wetting of soil in
 526 arid or semi-arid conditions ($P(l_{dry})$), as explained in section 2.1 (Equation 37). Denitrification
 527 NO is also calculated using the overall $r_{\text{NO}_x/\text{N}_2\text{O}}$ ratio (Equation 38) but does not experience
 528 pulsing (Parton et al., 2001). Equation 35 does quantify $r_{\text{NO}_x/\text{N}_2\text{O}}$ as a function of Dr , but as a
 529 unitless ratio as expected.

$$530 \quad r_{\text{NO}_x/\text{N}_2\text{O}} = 15.2 + \left(\frac{35.5 \arctan(0.68 \pi ((10.0 Dr) - 1.86))}{\pi} \right) \quad (35)$$

$$531 \quad N_{\text{N}_2\text{O}} (\text{Nitrification } \text{N}_2\text{O}, g - N/hr) = 0.02 (R_N) (\text{Grid cell area}) \quad (36)$$

$$532 \quad N_{\text{NO}_x} (\text{Nitrification } \text{NO}_x, g - N/hr) = r_{\text{NO}_x/\text{N}_2\text{O}} (N_{\text{N}_2\text{O}}) P(l_{dry}) \quad (37)$$

$$533 \quad D_{\text{NO}} (\text{Denitrification } \text{NO}, g - N/hr) = r_{\text{NO}_x/\text{N}_2\text{O}} (D_{\text{N}_2\text{O}}) \quad (38)$$

534 N_2O from denitrified NO_3 (R_D) is calculated using the partitioning function derived by Del Grosso
 535 et al. (2000) (Equation 39). The ratio of N_2 to N_2O emitted as an intermediate during denitrification
 536 ($r_{\text{N}_2/\text{N}_2\text{O}}$) is dependent on WFPS (Equation 42) and the relative availability of NO_3 substrate and
 537 C for heterotrophic respiration (Equations 40-41). The C available for heterotrophic respiration in
 538 the surface soil layer (LabileC) (Equation 41) is taken from EPIC for agricultural biomes and from
 539 Xu et al. (2015) for non-agricultural biomes. $f(\text{NO}_3:C)$ is controlled by variability in soil texture,
 540 accounted by a factor k , which depends on soil diffusivity at field capacity as estimated in Del
 541 Grosso et al. (2000). Also, the NO_3 pool is updated at each time step when denitrification happens
 542 (Equation 43). Equations 40-42 also quantify $r_{\text{N}_2/\text{N}_2\text{O}}$ as a unitless ratio, while still accounting for
 543 variables influencing these ratios.

$$544 \quad D_{\text{N}_2\text{O}} (\text{Denitrification } \text{N}_2\text{O}, g - N/hr) = \left(\frac{R_D}{1.0 + r_{\text{N}_2/\text{N}_2\text{O}}} \right) (\text{Grid cell area}) \quad (39)$$

$$545 \quad r_{\text{N}_2/\text{N}_2\text{O}} = f(\text{NO}_3:C) f(\text{WFPS}) \quad (40)$$

$$546 \quad f(\text{NO}_3:C) = \begin{cases} \max \left(0.16 (k), (k) e^{-0.8 \left(\frac{\text{NO}_3}{\text{LabileC}} \right)} \right), & \text{if } \text{LabileC} > 0 \\ 0.16 (k), & \text{if } \text{LabileC} \sim 0 \end{cases} \quad (41)$$

$$547 \quad f(\text{WFPS}) = \max \left(0.1, (0.015 (\text{WFPS}(\text{as fraction}) - 0.32)) \right) \quad (42)$$



548 NO_3 ($kg - N/ha$, after denitrification)

549
$$= \frac{R_N}{K_D} + \left(NO_3 - \frac{R_N}{K_D} \right) (e^{-(K_D dt)}) \quad (43)$$

550 HONO is emitted as an intermediate during nitrification, and has been reported in terms of a ratio
 551 relative to NO for each of 17 ecosystems by Oswald et al. (2013). In the mechanistic scheme, the
 552 proportions of HONO relative to total NO_x for these 17 biomes were mapped to the closest 24
 553 MODIS type biome categories (Table A1) and then to the NLCD 40 types ($HONO_f$) by the
 554 mappings in Tables A2 and A3. This allows consistency with sub-grid land use fractions from
 555 NLCD40. HONO emissions are further adjusted to reflect their dependence on WFPS (Oswald et
 556 al., 2013). The adjustment factor f_{SWC} reflects observations that HONO emissions rise linearly up
 557 to 10% WFPS and then decrease until they are negligible around ~ 40% (Su et al., 2011; Oswald
 558 et al., 2013) (Equation 45). Subsequently, total NO emission is a sum of nitrification NO emission,
 559 which is a difference of N_{NO_x} and S_{HONO} , and denitrification NO (Equation 46). Similarly, total
 560 N_2O is a sum of N_{N_2O} (Equation 36) and D_{N_2O} (Equation 39). The canopy reduction factor (section
 561 2.1) is then applied to both S_{HONO} and S_{NO} (Equations 44 and 46). Finally, sub-grid scale emission
 562 rates are aggregated for each grid cell.

563
$$S_{HONO} = (HONO_f)(N_{NO_x}) (f_{SWC})CRF(LAI, Meteorology, Biome) \quad (44)$$

564 f_{SWC} (Soil water content adjustment factor to compute HONO)

565
$$= \begin{cases} \frac{(HONO_f)(WFPS)}{0.1}, & \text{If } (WFPS \leq 0.10) \\ \text{(Assuming linear increase up to 10\% WFPS)} \\ \frac{(HONO_f)(0.4 - WFPS)}{(0.4 - 0.1)}, & \text{If } (WFPS \leq 0.40) \\ 0, & \text{If } (WFPS > 0.40) \end{cases} \quad (45)$$

566

567
$$S_{NO} = \left\{ \left(N_{NO_x} - \left((HONO_f)(N_{NO_x}) (f_{SWC}) \right) \right) \right.$$

568
$$\left. + D_{NO} \right\} CRF(LAI, Meteorology, Biome) \quad (46)$$

569



570 2.7 Model configurations

571 We obtained from U.S. EPA a base case WRFv3.7-CMAQv5.1 simulation for 2011 with the
572 settings and CONUS modeling domain described by Appel et al. (2017), who thoroughly evaluated
573 its performance against observations. Here, we simulate only May and July to test sensitivity of
574 air pollution to soil N emissions during the beginning and middle of the growing season. Each
575 episode is preceded by a 10-day spin-up period.

576 Table 2 summarizes the WRF-CMAQ modeling configurations settings. The simulations use the
577 Pleim-Xiu Land Surface Model (PX-LSM) (Pleim and Xiu, 2003) and the Asymmetric Convective
578 Mixing v2 (ACM2) Planetary Boundary Layer (PBL) model. The modeling domain for CMAQ
579 v5.1 covers the entire CONUS including portions of northern Mexico and southern Canada with
580 12-km resolution and a Lambert Conformal projection. Vertically, we use 35 vertical layers of
581 increasing thickness extending up to 50 hPa. Boundary conditions are provided by a 2011 global
582 GEOS-Chem simulation (Bey et al., 2001).

583 WRF simulations employed the same options as Appel et al. (2017) (Summarized in Table 2).
584 WRF outputs for meteorological conditions were converted to CMAQ inputs using MCIP version
585 4.2 (<https://www.cmascenter.org>). Gridded speciated hourly model-ready emissions inputs were
586 generated using Sparse Matrix Operator Kernel Emissions (SMOKE;
587 <https://www.cmascenter.org/smoke/>) version 3.5 program and the 2011 National Emissions
588 Inventory v1. Biogenic emissions were processed in-line in CMAQ v5.1 using BEIS version 3.61
589 (Bash et al., 2016). All the simulations employed the bidirectional option for estimating the air–
590 surface exchange of ammonia. We applied CMAQ with three sets of soil NO emissions: a)
591 standard YL soil NO scheme in BEIS; b) updated BDSNP scheme for NO (Rasool et al., 2016)
592 with new sub-grid biome classification; and c) mechanistic soil N scheme for NO and HONO.

593

594 2.8 Observational data for model evaluation

595 To evaluate model performance for each of the three soil N cases, we employed regional and
596 national networks: EPA's Air Quality System (AQS; 2086 sites; <https://www.epa.gov/aqs>) for
597 hourly NO_x and O₃; the Interagency Monitoring of Protected Visual Environments (IMPROVE;
598 157 sites; <http://vista.cira.colostate.edu/improve/>) and Chemical Speciation Network (CSN; 171



599 sites; <https://www3.epa.gov/ttnamti1/speciepg.html>) for PM_{2.5} nitrate (measured every third or
600 sixth day); the Clean Air Status and Trends Network (CASTNET; 82 sites; [http://](http://www.epa.gov/castnet/)
601 www.epa.gov/castnet/) for hourly O₃ and weekly aerosol PM species; and SEARCH network
602 measurements (<http://www.atmospheric-research.com/studies/SEARCH/index.html>) of NO_x
603 concentrations in remote areas. NO₂ was also evaluated against tropospheric columns observed by
604 the Ozone Monitoring Instrument (OMI) aboard NASA's Aura satellite (Bucsela et al., 2013;
605 Lamsal et al., 2014).

606

607 **3 Results and Discussion**

608 **3.1 Spatial distribution of soil NO, HONO and N₂O emissions**

609 Figure 3 compares the spatial distribution of soil N oxide emissions from the three schemes. The
610 incorporation of EPIC fertilizer in BDSNP results in soil NO emission rates up to a factor of 1.5
611 higher than in YL, consistent with the findings of Rasool et al. (2016). Hudman et al. (2012) found
612 nearly twice as large of a gap between BDSNP and YL in GEOS-Chem; the narrower gap here
613 likely results from our use of sub-grid biome classification and EPIC fertilizer data. The
614 mechanistic scheme (Figure 3c) generates emission estimates that are closer to the YL scheme but
615 with greater spatial and temporal heterogeneity, reflecting its more dynamic soil N and C pools.
616 The agricultural plains extending from Iowa to Texas with high fertilizer application rates have
617 the highest biogenic NO and HONO emission rate, with obvious temporal variability between May
618 and July (Figure 3). In all of the schemes, soil N represents a substantial fraction of total NO_x
619 emissions over many rural regions, especially in the western half of the country (Figure S1).
620 However, the aggregated budget of soil NO is much less than anthropogenic NO_x, because
621 anthropogenic emissions are concentrated in a limited number of urbanized and industrial
622 locations. The percentage contribution of soil NO to total NO_x aggregated across the CONUS
623 domain varied for May-July between: 15-20% for YL, 20-33% for updated BDSNP, and 10-13%
624 for mechanistic schemes respectively.

625 Direct observations of soil emissions are sparse and most were reported decades ago. While the
626 meteorological conditions will differ, these observations give us the best available indicator of the
627 ranges of magnitudes of emission rates actually observed in the field. The sites encompass a variety



628 of fertilized agricultural fields and fertilized and unfertilized grasslands (Bertram et al., 2005;
629 Hutchinson and Brams, 1992; Parrish et al., 1987; Williams et al., 1991; Williams et al., 1992;
630 Martin et al., 1998). For fair comparison, peak location/site was selected across a range of sites for
631 a specific observation study and compared to respective peak modeled value across sites/grids in
632 the same spatial domain. Also, for comparison with natural unfertilized grassland observational
633 studies based in Colorado, modeled estimates from non-agricultural grids only were selected.
634 Overall, the YL scheme and the mechanistic scheme produce emissions estimates that are roughly
635 consistent with the ranges of emission rates observed at each site (Table 3). By contrast, BDSNP
636 tends to overestimate soil NO compared to these observations (Table 3).

637 Table 3 also shows opposing trends for May and July soil NO estimates between YL or BDSNP
638 and mechanistic schemes for Iowa and South Dakota fertilized fields that make up the significant
639 part of corn-belt in U.S. For these regions, soil NO tends to be higher in July than in May in YL
640 and BDSNP, but lower in July in the mechanistic scheme (Table 3). The U.S. Corn Belt has the
641 most synthetic N fertilizer application in April (Wade et al., 2015), which can explain the high soil
642 NO emissions in May that decline in July. N₂O emissions have been particularly observed to be
643 highest during May-June after April N fertilizer application in the U.S. Corn Belt, and declining
644 thereafter (Griffis et al., 2017). This is further confirmed in our estimates for soil N₂O emissions
645 from mechanistic scheme, where May estimates are higher than in July and the maximum
646 emissions are observed in the Iowa Corn Belt (Figure 4). However, unlike NO_x emissions, for N₂O
647 no background conditions or emission inventory is in place in CMAQ's chemical transport model,
648 so comparisons with ambient observations are not yet possible.

649

650 **3.2 Evaluation with PM_{2.5}, ozone, and NO_x observations**

651 Model results with the three soil N schemes are compared with observational data from IMPROVE
652 and CSN monitors for PM_{2.5} NO₃ component, AQS monitors for NO_x and ozone, and CASTNET
653 monitors for ozone. Both YL and the new mechanistic schemes exhibit similar ranges of biases for
654 these pollutants (see Figures S2, S3, S4, S5 and S6 in supplementary material). Use of the
655 mechanistic scheme in place of YL changes soil N emissions by less than 25 ng-N m⁻² s⁻¹ in most



656 regions, corresponding to NO_x concentration changes of less than 1 ppb (Figure 5). CASTNET
657 and IMPROVE monitors tend to be more remote than AQS and CSN monitors, many of which are
658 located in urban regions.

659 At AQS monitors, switching between soil N schemes changes MB for O_3 by up to ~ 1.5 ppb (Figure
660 6), whereas absolute MB of models versus observations is up to ~ 10 ppb (Figure S2). For NO_x ,
661 the maximum difference in MB between soil N schemes is ~ 0.4 ppb (Figure 7), compared to
662 maximum absolute MB of ~ 10 ppb between model and observations (Figure S3). For CASTNET
663 monitors, the differences in MB for O_3 between soil N schemes can reach a maximum of ~ 1.5 ppb
664 (Figure 8), compared to 6 ppb maximum absolute MB of models versus observations (Figure S4).
665 Similarly, for IMPROVE $\text{PM}_{2.5}$ NO_3 , maximum difference in MB between soil N schemes is \sim
666 $0.06 \mu\text{g}/\text{m}^3$ (Figure 9), compared to maximum absolute MB of $0.4 \mu\text{g}/\text{m}^3$ (Figure S5). For CSN
667 $\text{PM}_{2.5}$ NO_3 , the maximum MB difference between soil N schemes is $\sim 0.1 \mu\text{g}/\text{m}^3$ (Figure 10),
668 compared to maximum absolute MB of $\sim 50 \mu\text{g}/\text{m}^3$ (Figure S6). Similar trends are observed for
669 both May and July as illustrated in Figures 6-10.

670 Overall, the mechanistic scheme tends to reduce CMAQ's positive biases for pollutants across the
671 Midwest and eastern US, whereas BDSNP worsens overestimations in these regions for both May
672 and July 2011 (Figures 6-10). One reason for the differences is that the mechanistic scheme
673 recognizes dry conditions in unirrigated fields in these regions, whereas the low WFPS threshold
674 in BDSNP ($\theta = 0.175 (\text{m}^3/\text{m}^3)$) treats most of these regions as wet and thus higher emitting.

675 **3.2.1 Evaluation with South Eastern Aerosol Research and CHaracterization** 676 **(SEARCH) Network NO_x measurements**

677 We analyzed how the choice of soil NO parameterization affects NO_x concentrations in non-
678 agricultural regions by using SEARCH network measurements ([http://www.atmospheric-
679 research.com/studies/SEARCH/index.html](http://www.atmospheric-research.com/studies/SEARCH/index.html)). Six SEARCH sites located in the southeastern U.S.
680 are evaluated for May and July 2011: Gulfport, Mississippi (GFP) urban coastal site ~ 1.5 km from
681 the shoreline, Pensacola – outlying (aircraft) landing field (OLF) remote coastal site near the Gulf
682 ~ 20 km inland, Atlanta, Georgia–Jefferson Street (JST) and North Birmingham, Alabama (BHM);



683 both urban inland sites, and Yorkville, Georgia (YRK) and Centreville, Alabama (CTR), remote
684 inland forest sites.

685 Across the southeastern U.S. during these episodes, BDSNP estimated higher emissions than YL
686 and the mechanistic scheme estimated lower emissions (Figure 3). Also, CMAQ with each scheme
687 overestimated NO_x observed at each SEARCH site (Figure 11). Thus, shifting from YL to BDSNP
688 worsens mean bias (MB) for NO_x , while the mechanistic scheme reduces MB. The impacts are
689 most pronounced at the rural Centerville site (Figure 11).

690

691 **3.3 Evaluation with OMI satellite NO_2 column observations**

692 Tropospheric NO_2 columns observed by OMI and available publicly at the NASA archive
693 (http://disc.sci.gsfc.nasa.gov/Aura/data-holdings/OMI/omno2_v003.shtml; Bucsele et al., 2013;
694 Lamsal et al., 2014) are used to evaluate the performance of CMAQ under the three soil NO_x
695 schemes. To enable a fair comparison, the quality-assured/quality-checked (QA/QC) clear-sky
696 (cloud radiance fraction < 0.5) OMI NO_2 data are gridded and projected to our CONUS domain
697 using ArcGIS 10.3.1. CMAQ NO_2 column densities in molecules per cm^2 are generated from
698 CMAQ through vertical integration using the variable layer heights and air mass densities in these
699 tropospheric layers. These NO_2 column densities are then extracted for 13:00-14:00 local time
700 across the CONUS domain, to match the time of OMI overpass measurements.

701 We compared CMAQ simulated tropospheric NO_2 columns with OMI data for four broad regions
702 that showed the highest sensitivity to the soil N schemes. For May 2011, the mechanistic scheme
703 produces higher estimates of NO_2 than YL in the western U.S. and Texas, and lower estimates in
704 the rest of the agricultural Great Plains. In July however, the mechanistic scheme produces lower
705 estimates than YL in each of these regions, but the differences are narrower than in May (Figure
706 12). Switching from YL to our updated mechanistic scheme improved agreement with OMI NO_2
707 columns in the western U.S. (for May only), Montana, North and South Dakota, North and South
708 Carolina and Georgia (July only), and Oklahoma and Texas (red boundaries). However, switching
709 from YL to mechanistic scheme worsens underpredictions of column NO_2 in the rest of the
710 Midwest (black boundaries) during both May and July (Figures 12 and 13). The mechanistic
711 scheme improves model performance in the southeastern U.S. and many portions of the central



712 and western U.S. (Table 4). Overestimation is exhibited for the eastern U.S. across all soil N
713 schemes and can be attributed more to the current emission inventory in CMAQ overestimating
714 NO₂ vertical column density in this region of CONUS (Kim et al., 2016). For Texas and Oklahoma,
715 the mechanistic scheme performs better than YL but still underestimates OMI observations in
716 May, and performs well in July (Figure 13).

717 Underestimates of soil N in some regions may be attributed to the lack of representation of farm-
718 level manure N management practices, in which manure application can exceed the EPIC estimate
719 of optimal crop demand. Farms in the vicinity of concentrated animal units often apply N in excess
720 of the crop N requirements as part of the manure management strategy, typically increasing the N
721 emissions (Montes et al., 2013). USDA has reported that confined animal units/livestock
722 production correlates with increasing amounts of farm-level excess N (Kellogg et al., 2000;
723 Ribaudo and Sneeringer, 2016). Model representations of these practices are needed to better
724 estimate the impact of nitrogen in the environment.

725

726 **4 Conclusions**

727 Our implementation of a mechanistic scheme for soil N emissions in CMAQ provides a more
728 physically based representation of soil N than previous parametric schemes. To our knowledge,
729 this is the first time that soil biogeochemical processes and emissions across a full range of nitrogen
730 compounds have been simulated in a physically realistic manner in a regional photochemical
731 model. Our mechanistic scheme directly simulates nitrification and denitrification processes,
732 allowing it to consistently estimate soil emissions of NO, HONO, NH₃, and N₂O (Figures 1 and
733 2). The mechanistic scheme also updates the representation of the dependency of soil N on WFPS
734 by utilizing parameters like water content at saturation, wilting point, and field capacity and their
735 impact on gas diffusivity (Del Grosso et al., 2000; Parton et al., 2001).

736 Overall, the magnitudes of soil NO_x emissions predicted by the mechanistic scheme are similar to
737 those predicted by the YL parametric scheme, and smaller than those predicted by the BDSNP
738 scheme. In dry conditions, soil NO has been shown to be highest as compared to wet conditions
739 with lowest, explained by sustained high nitrification rates due to high gas diffusivity in dry



740 conditions (Homyak et al., 2014). Arid soils or dry season with adequate soil N due to asynchrony
741 between soil C mineralization and nitrification have been shown to shut down plant N uptake
742 through high gas diffusivity, causing NO emissions to increase (Evans and Burke, 2013; Homyak
743 et al., 2016). Mechanistic scheme exhibits this spatial variability in soil NO depending on dry or
744 wet conditions, since it accounts for their dependence on soil moisture and gas diffusivity, as well
745 as the C and N cycling that leads to adequate soil N.

746 Spatial patterns of NO_x emissions differ across the schemes and episodes (Figure 3), but generally
747 show highest emissions in fertilized agricultural regions. During the episodes considered here,
748 Texas experienced severe to extreme drought, while parts of the Northeast and Pacific Northwest
749 were unusually wet
750 (http://www.cpc.ncep.noaa.gov/products/analysis_monitoring/regional_monitoring/palmer/2011/
751). Testing for other time periods is needed to see how results differ during different seasons and as
752 drought conditions vary. Model evaluation will also depend on the meteorological model's skill in
753 capturing dry and wet conditions.

754 The lower emissions of the mechanistic scheme reduce the overprediction biases for ground-based
755 observations of ozone and PM nitrate that had been reported by Rasool et al. (2016) for the BDSNP
756 scheme (Figures 6-10). The mechanistic scheme reduced overpredictions of NO_x concentrations
757 at SEARCH sites in the southeastern U.S. (Figure 11). However, changes in performance for
758 simulating satellite observations of NO₂ columns were mixed (Figures 12-13). The
759 underestimation of NO₂ by CMAQ with the mechanistic scheme in agricultural regions of the
760 Midwest may be partially attributed to neglecting manure management practices from livestock
761 operations.

762 Although this work represents the most process-based representation of soil N ever introduced to
763 a regional photochemical model, limitations remain. EPIC still lacks complete representation of
764 farming management practices like excess N applied as part of nutrient management from
765 livestock, which can increase soil N pools and associated emissions. Developing and evaluating
766 these models to addresses management decisions is challenging as they are often regionally
767 specific and based on expert knowledge including regional and global economics and
768 biogeochemical processes that have yet to be codified into a predictive system. Some aspects of



769 soil N biogeochemistry remain insufficiently understood, especially as they relate to HONO
770 emissions. Nevertheless, the mechanistic approach introduced here will make it possible to
771 incorporate future advancements in understanding C and N cycling processes.

772 For future work, there is a need for more accurate representation of actual farming practices beyond
773 the generalizations made by the EPIC model. Model development should be continued to better
774 constrain N sources such as rock weathering, which are still ignored for estimating soil N
775 emissions. Recently, Houlton et al. (2018) postulated that bedrock weathering can contribute an
776 additional 6-17 % to global inorganic soil N for different natural biomes. There is also a need for
777 more field observations of soil N emissions to better evaluate the spatial and temporal patterns
778 simulated by the models.

779

780 **Code availability**

781 The modified and new source code, inputs, and sample outputs along with the user manual giving
782 details on implementing the new mechanistic module in-line with CMAQ Version 5.1, as used in
783 this work are available on the Oak Ridge National Laboratory Distributed Active Archive Center
784 for Bio-geochemical Dynamics (Rasool et al., 2018; <https://doi.org/10.3334/ORNLDAAC/1661>).
785 Source codes for CMAQ version 5.1 and FEST-C version 1.2 are both open-source, available with
786 applicable free registration at <http://www.cmascenter.org>. Advanced Research WRF model
787 (ARW) version 3.7 used in this study is also available as a free open-source resource at
788 http://www2.mmm.ucar.edu/wrf/users/download/get_source.html.

789

790 **Author contribution**

791 Quazi Rasool developed the model code with Jesse Bash. Quazi Rasool performed the simulations
792 and analysis. Quazi Rasool prepared the manuscript with extensive reviews and edits from Jesse
793 Bash and Daniel Cohan.



794

795 **Acknowledgements**

796 NASA (grant number NNX15AN63G) provided the funding for this work. We acknowledge Dr.

797 Ellen Cooter from U.S. EPA for her insights and invaluable help with EPIC/FEST-C modeling.

798 The views expressed in this article are those of the authors and do not necessarily reflect the views

799 or policies of the U.S. Environmental Protection Agency.



800 **References**

- 801 Appel, K. W., Napelenok, S. L., Foley, K. M., Pye, H. O., Hogrefe, C., Luecken, D. J., Bash, J.
802 O., Roselle, S. J., Pleim, J. E., and Foroutan, H.: Description and evaluation of the Community
803 Multiscale Air Quality (CMAQ) modeling system version 5.1, Geoscientific Model Development,
804 10, 1703, 2017.
- 805 Barton, L., McLay, C., Schipper, L., and Smith, C.: Annual denitrification rates in agricultural and
806 forest soils: a review, *Soil Research*, 37, 1073-1094, 1999.
- 807 Bash, J. O., Baker, K. R., and Beaver, M. R.: Evaluation of improved land use and canopy
808 representation in BEIS v3. 61 with biogenic VOC measurements in California, Geoscientific
809 Model Development, 9, 2191, 2016.
- 810 Bash, J., Cooter, E., Dennis, R., Walker, J., and Pleim, J.: Evaluation of a regional air-quality
811 model with bidirectional NH₃ exchange coupled to an agroecosystem model, *Biogeosciences*, 10,
812 1635-1645, 2013.
- 813 Bertram, T. H., Cohen, R. C., Thorn III, W. J., and Chu, P. M.: Consistency of ozone and nitrogen
814 oxides standards at tropospherically relevant mixing ratios, *Journal of the Air & Waste
815 Management Association*, 55, 1473-1479, 2005.
- 816 Bey, I., Jacob, D. J., Yantosca, R. M., Logan, J. A., Field, B., Fiore, A. M., Li, Q., Liu, H., Mickley,
817 L. J., and Schultz, M.: Global modeling of tropospheric chemistry with assimilated meteorology:
818 Model description and evaluation, *J. Geophys. Res.*, 106, 23,073-23,096, 2001.
- 819 Bucsel, E. J., Krotkov, N. A., Celarier, E. A., Lamsal, L. N., Swartz, W. H., Bhartia, P. K.,
820 Boersma, K. F., Veefkind, J. P., Gleason, J. F., and Pickering, K. E.: A new stratospheric and
821 tropospheric NO₂ retrieval algorithm for nadir-viewing satellite instruments: applications to OMI,
822 *Atmos. Meas. Tech.*, 6, 2607-2626, doi:10.5194/amt-6-2607-2013, 2013.
- 823 Butterbach-Bahl, K., Baggs, E. M., Dannenmann, M., Kiese, R., and Zechmeister-Boltenstern, S.:
824 Nitrous oxide emissions from soils: how well do we understand the processes and their controls?,
825 *Phil. Trans. R. Soc. B*, 368, 20130122, 2013.



- 826 Cameron, K., Di, H. J., and Moir, J.: Nitrogen losses from the soil/plant system: a review, *Annals*
827 *of Applied Biology*, 162, 145-173, 2013.
- 828 Conrad, R.: Microbiological and biochemical background of production and consumption of NO
829 and N₂O in soil. In: *Trace gas exchange in forest ecosystems*, Springer, 2002.
- 830 Cooper, O.R., Parrish, D.D., Ziemke, J., Balashov, N.V., Cupeiro, M., Galbally, I.E., Gilge, S.,
831 Horowitz, L., Jensen, N.R., Lamarque, J.F. and Naik, V.: Global distribution and trends of
832 tropospheric ozone: An observation-based review. *Elementa: Science of the Anthropocene*, 2(1),
833 p.000029, 2014.
- 834 Cooter, E., Bash, J., Benson, V., and Ran, L.: Linking agricultural crop management and air quality
835 models for regional to national-scale nitrogen assessments, *Biogeosciences*, 9, 4023-4035, 2012.
- 836 Davidson, E. A. and Verchot, L. V.: Testing the Hole-in-the-Pipe Model of nitric and nitrous oxide
837 emissions from soils using the TRAGNET Database, *Global Biogeochemical Cycles*, 14, 1035-
838 1043, 2000.
- 839 Davidson, E. and Kinglerlee, W.: A global inventory of nitric oxide emissions from soils, *Nutr.*
840 *Cycl. Agroecosys.*, 48, 37–50, doi:10.1023/A:1009738715891, 1997.
- 841 Davidson, E., David, M. B., Galloway, J. N., Goodale, C. L., Haeuber, R., Harrison, J. A.,
842 Howarth, R. W., Jaynes, D. B., Lowrance, R. R., and Thomas, N. B.: Excess nitrogen in the US
843 environment: trends, risks, and solutions, *Issues in Ecology*, 2011. 2011.
- 844 Davidson, E.: Pulses of nitric oxide and nitrous oxide flux following wetting of dry soil: an
845 assessment of probable sources and importance relative to annual fluxes, *Ecol. Bull.*, 42, 149–155,
846 1992.
- 847 Del Grosso, S., Parton, W., Mosier, A., Ojima, D., Kulmala, A., and Phongpan, S.: General model
848 for N₂O and N₂ gas emissions from soils due to denitrification, *Global Biogeochemical Cycles*,
849 14, 1045-1060, 2000.
- 850 Dinnes, D. L., Karlen, D. L., Jaynes, D. B., Kaspar, T. C., Hatfield, J. L., Colvin, T. S., and
851 Cambardella, C. A.: Nitrogen management strategies to reduce nitrate leaching in tile-drained
852 Midwestern soils, *Agronomy journal*, 94, 153-171, 2002.



- 853 Evans, S. E. and Burke, I. C.: Carbon and nitrogen decoupling under an 11-year drought in the
854 shortgrass steppe, *Ecosystems*, 16, 20-33, 2013.
- 855 Firestone, M. K. and Davidson, E. A.: Microbiological basis of NO and N₂O production and
856 consumption in soil, *Exchange of trace gases between terrestrial ecosystems and the atmosphere*,
857 47, 7-21, 1989.
- 858 Frink, C. R., Waggoner, P. E., and Ausubel, J. H.: Nitrogen fertilizer: retrospect and prospect,
859 *Proceedings of the National Academy of Sciences*, 96, 1175-1180, 1999.
- 860 Gaillard, R. K., Jones, C. D., Ingraham, P., Collier, S., Izaurralde, R. C., Jokela, W., Osterholz,
861 W., Salas, W., Vadas, P., and Ruark, M.: Underestimation of N₂O emissions in a comparison of
862 the DayCent, DNDC, and EPIC models, *Ecological Applications*, 2017. 2017.
- 863 Geddes, J. A., Heald, C. L., Silva, S. J., and Martin, R. V.: Land cover change impacts on
864 atmospheric chemistry: simulating projected large-scale tree mortality in the United States,
865 *Atmospheric Chemistry and Physics*, 16, 2323-2340, 2016.
- 866 Gödde, M. and Conrad, R.: Influence of soil properties on the turnover of nitric oxide and nitrous
867 oxide by nitrification and denitrification at constant temperature and moisture, *Biology and
868 Fertility of Soils*, 32, 120-128, 2000.
- 869 Griffis, T. J., Chen, Z., Baker, J. M., Wood, J. D., Millet, D. B., Lee, X., Venterea, R. T., and
870 Turner, P. A.: Nitrous oxide emissions are enhanced in a warmer and wetter world, *Proceedings
871 of the National Academy of Sciences*, 114, 12081-12085, 2017.
- 872 Heil, J., Vereecken, H., and Brüggemann, N.: A review of chemical reactions of nitrification
873 intermediates and their role in nitrogen cycling and nitrogen trace gas formation in soil, *European
874 journal of soil science*, 67, 23-39, 2016.
- 875 Hickman, J. E., Wu, S., Mickley, L. J., and Lerdau, M. T.: Kudzu (*Pueraria montana*) invasion
876 doubles emissions of nitric oxide and increases ozone pollution, *Proceedings of the National
877 Academy of Sciences*, 107, 10115-10119, 2010. Holmes, N. S.: A review of particle formation
878 events and growth in the atmosphere in the various environments and discussion of mechanistic
879 implications, *Atmospheric Environment*, 41, 2183-2201, 2007.



- 880 Homyak, P. M. and Sickman, J. O.: Influence of soil moisture on the seasonality of nitric oxide
881 emissions from chaparral soils, Sierra Nevada, California, USA, *Journal of arid environments*,
882 103, 46-52, 2014.
- 883 Homyak, P. M., Blankinship, J. C., Marchus, K., Lucero, D. M., Sickman, J. O., and Schimel, J.
884 P.: Aridity and plant uptake interact to make dryland soils hotspots for nitric oxide (NO) emissions,
885 *Proceedings of the National Academy of Sciences*, 113, E2608-E2616, 2016.
- 886 Houlton, B., Morford, S., and Dahlgren, R.: Convergent evidence for widespread rock nitrogen
887 sources in Earth's surface environment, *Science*, 360, 58-62, 2018.
- 888 Hudman, R. C., Moore, N. E., Mebust, A. K., Martin, R. V., Russell, A. R., Valin, L. C., and
889 Cohen, R. C.: Steps towards a mechanistic model of global soil nitric oxide emissions:
890 implementation and space based-constraints, *Atmos. Chem. Phys.*, 12, 7779– 7795,
891 doi:10.5194/acp-12-7779-2012, 2012.
- 892 IPCC: *Climate Change 2007: Impacts, Adaptation and Vulnerability, Contribution of Working*
893 *Group II to the Fourth Assessment Report of the Intergovernmental Panel on Climate Change*,
894 edited by: Parry, M. L., Canziani, O. F., Palutikof, J. P., van der Linden, P. J., and Hanson, C. E.,
895 Cambridge University Press, Cambridge, UK, 976 pp., 2007.
- 896 Hudman, R. C., Russell, A. R., Valin, L. C., and Cohen, R. C.: Interannual variability in soil nitric
897 oxide emissions over the United States as viewed from space, *Atmos. Chem. Phys.*, 10, 9943–
898 9952, doi:10.5194/acp-10-9943-2010, 2010.
- 899 Hutchinson, G. and Brams, E.: NO versus N₂O emissions from an NH₄⁺-amended Bermuda grass
900 pasture, *Journal of Geophysical Research: Atmospheres*, 97, 9889-9896, 1992.
- 901 Izaurrealde, R. C., McGill, W. B., and Williams, J.: Development and application of the EPIC model
902 for carbon cycle, greenhouse gas mitigation, and biofuel studies. In: *Managing Agricultural*
903 *Greenhouse Gases*, Elsevier, 2012.
- 904 Izaurrealde, R., Williams, J. R., McGill, W. B., Rosenberg, N. J., and Jakas, M. Q.: Simulating soil
905 C dynamics with EPIC: Model description and testing against long-term data, *Ecological*
906 *Modelling*, 192, 362-384, 2006.



- 907 Jaeglé, L., Martin, R. V., Chance, K., Steinberger, L., Kurosu, T. P., Jacob, D. J., Modi, A. I.,
908 Yoboué, V., Sigha-Nkamdjou, L., and Galy-Lacaux, C.: Satellite mapping of rain-induced nitric
909 oxide emissions from soils, *J. Geophys. Res.-Atmos.*, 109, D21310, doi:10.1029/2004JD004787,
910 2004.
- 911 Jaeglé, L., Steinberger, L., Martin, R. V., and Chance, K.: Global partitioning of NO_x sources
912 using satellite observations: Relative roles of fossil fuel combustion, biomass burning and soil
913 emissions, *Faraday Discussions*, 130, 407-423, 2005.
- 914 Kampa, M. and Castanas, E.: Human health effects of air pollution, *Environmental pollution*, 151,
915 362-367, 2008.
- 916 Kellogg, R. L., Lander, C. H., Moffitt, D. C., and Gollehon, N.: Manure nutrients relative to the
917 capacity of cropland and pastureland to assimilate nutrients: Spatial and temporal trends for the
918 United States, *Proceedings of the Water Environment Federation*, 2000, 18-157, 2000.
- 919 Kesik, M., Blagodatsky, S., Papen, H., and Butterbach-Bahl, K.: Effect of pH, temperature and
920 substrate on N₂O, NO and CO₂ production by *Alcaligenes faecalis* p, *Journal of applied*
921 *microbiology*, 101, 655-667, 2006.
- 922 Kim, H. C., Lee, P., Judd, L., Pan, L., and Lefer, B.: OMI NO₂ column densities over North
923 American urban cities: the effect of satellite footprint resolution, *Geoscientific Model*
924 *Development*, 9, 2016.
- 925 Kottek, M., Grieser, J., Beck, C., Rudolf, B., and Rubel, F.: World Map of the Köppen-Geiger
926 climate classification updated. *Meteorologische Zeitschrift*, 15, 259-263. DOI: 10.1127/0941-
927 2948/2006/0130, 2006.
- 928 Kwok, R., Napelenok, S., and Baker, K.: Implementation and evaluation of PM_{2.5} source
929 contribution analysis in a photochemical model, *Atmospheric environment*, 80, 398-407, 2013.
- 930 Lamsal, L., Krotkov, N., Celarier, E., Swartz, W., Pickering, K., Bucsela, E., Gleason, J., Martin,
931 R., Philip, S., and Irie, H.: Evaluation of OMI operational standard NO₂ column retrievals using
932 in situ and surface-based NO₂ observations, *Atmospheric Chemistry and Physics*, 14, 11587-
933 11609, 2014.



- 934 Laville, P., Lehuger, S., Loubet, B., Chaumartin, F., and Cellier, P.: Effect of management, climate
935 and soil conditions on N₂O and NO emissions from an arable crop rotation using high temporal
936 resolution measurements, *Agricultural and Forest Meteorology*, 151, 228-240, 2011.
- 937 Leitner, S., Homyak, P. M., Blankinship, J. C., Eberwein, J., Jenerette, G. D., Zechmeister-
938 Boltenstern, S., and Schimel, J. P.: Linking NO and N₂O emission pulses with the mobilization
939 of mineral and organic N upon rewetting dry soils, *Soil Biology and Biochemistry*, 115, 461-466,
940 2017.
- 941 Li, Y., Schichtel, B. A., Walker, J. T., Schwede, D. B., Chen, X., Lehmann, C. M., Puchalski, M.
942 A., Gay, D. A., and Collett, J. L.: Increasing importance of deposition of reduced nitrogen in the
943 United States, *Proceedings of the National Academy of Sciences*, 113, 5874-5879, 2016.
- 944 Liu, B., Mørkved, P. T., Frostegård, Å., and Bakken, L. R.: Denitrification gene pools,
945 transcription and kinetics of NO, N₂O and N₂ production as affected by soil pH, *FEMS*
946 *microbiology ecology*, 72, 407-417, 2010.
- 947 Liu, X., Ju, X., Zhang, Y., He, C., Kopsch, J., and Fusuo, Z.: Nitrogen deposition in
948 agroecosystems in the Beijing area, *Agriculture, ecosystems & environment*, 113, 370-377, 2006.
- 949 Lu, C. and Tian, H.: Global nitrogen and phosphorus fertilizer use for agriculture production in
950 the past half century: shifted hot spots and nutrient imbalance, *Earth System Science Data*, 9, 181,
951 2017.
- 952 Ludwig, J., Meixner, F., Vogel, B., and Förstner, J.: Soil-air exchange of nitric oxide: an overview
953 of processes, environmental factors, and modeling studies, *Biogeochemistry*, 52, 225-257,
954 doi:10.1023/A:1006424330555, 2001.
- 955 Machefer, S., Dise, N., Goulding, K., and Whitehead, P.: Nitrous oxide emission from a range of
956 land uses across Europe, *Hydrology and Earth System Sciences Discussions*, 6, 325-338, 2002.
- 957 Maljanen, M., Yli-Pirilä, P., Hytönen, J., Joutsensaari, J., and Martikainen, P. J.: Acidic northern
958 soils as sources of atmospheric nitrous acid (HONO), *Soil Biology and Biochemistry*, 67, 94-97,
959 2013.



- 960 Malm, W. C., Sisler, J. F., Huffman, D., Eldred, R. A., and Cahill, T. A.: Spatial and seasonal
961 trends in particle concentration and optical extinction in the United States, *Journal of Geophysical*
962 *Research: Atmospheres*, 99, 1347-1370, 1994.
- 963 Mamtimin, B., Meixner, F. X., Behrendt, T., Badawy, M., and Wagner, T.: The contribution of
964 soil biogenic NO and HONO emissions from a managed hyperarid ecosystem to the regional NO
965 x emissions during growing season, *Atmospheric Chemistry and Physics*, 16, 10175-10194, 2016.
- 966 Manzoni, S. and Porporato, A.: Soil carbon and nitrogen mineralization: theory and models across
967 scales, *Soil Biology and Biochemistry*, 41, 1355-1379, 2009.
- 968 Martin, R. E., Scholes, M., Mosier, A., Ojima, D., Holland, E., and Parton, W.: Controls on annual
969 emissions of nitric oxide from soils of the Colorado shortgrass steppe, *Global Biogeochemical*
970 *Cycles*, 12, 81-91, 1998.
- 971 Medinets, S., Skiba, U., Rennenberg, H., and Butterbach-Bahl, K.: A review of soil NO
972 transformation: Associated processes and possible physiological significance on organisms, *Soil*
973 *Biology and Biochemistry*, 80, 92-117, 2015.
- 974 Moldrup, P., Olesen, T., Yoshikawa, S., Komatsu, T., and Rolston, D. E.: Three-porosity model
975 for predicting the gas diffusion coefficient in undisturbed soil, *Soil Science Society of America*
976 *Journal*, 68, 750-759, 2004.
- 977 Montes, F., Meinen, R., Dell, C., Rotz, A., Hristov, A., Oh, J., Waghorn, G., Gerber, P., Henderson,
978 B., and Makkar, H.: SPECIAL TOPICS—mitigation of methane and nitrous oxide emissions from
979 animal operations: II. A review of manure management mitigation options, *Journal of Animal*
980 *Science*, 91, 5070-5094, 2013.
- 981 Necpálová, M., Anex, R. P., Fienen, M. N., Del Grosso, S. J., Castellano, M. J., Sawyer, J. E.,
982 Iqbal, J., Pantoja, J. L., and Barker, D. W.: Understanding the DayCent model, *Environmental*
983 *Modelling & Software*, 66, 110-130, 2015.
- 984 Neira, M.: The 2014 WHO conference on health and climate. *SciELO Public Health*, 2014.
- 985 Oikawa, P., Ge, C., Wang, J., Eberwein, J., Liang, L., Allsman, L., Grantz, D., and Jenerette, G.:
986 Unusually high soil nitrogen oxide emissions influence air quality in a high-temperature
987 agricultural region, *Nature communications*, 6, 8753, 2015.



- 988 Otte, T. L. and Pleim, J. E.: The Meteorology-Chemistry Interface Processor (MCIP) for the
989 CMAQ modeling system: updates through MCIPv3.4.1, *Geosci. Model Dev.*, 3, 243-256,
990 doi:10.5194/gmd-3-243-2010, 2010.
- 991 Parrish, D., Williams, E., Fahey, D., Liu, S., and Fehsenfeld, F.: Measurement of nitrogen oxide
992 fluxes from soils: Intercomparison of enclosure and gradient measurement techniques, *Journal of*
993 *Geophysical Research: Atmospheres*, 92, 2165-2171, 1987.
- 994 Parton, W. J., Holland, E. A., Del Grosso, S. J., Hartman, M. D., Martin, R. E., Mosier, A. R.,
995 Ojima, D. S., and Schimel, D. S.: Generalized model for NO_x and N₂O emissions from soils, *J.*
996 *Geophys. Res.-Atmos.*, 106, 17403–17419, doi:10.1029/2001JD900101, 2001.
- 997 Parton, W. J., Ojima, D. S., Cole, C. V., and Schimel, D. S.: A general model for soil organic
998 matter dynamics: sensitivity to litter chemistry, texture and management, *Quantitative modeling*
999 *of soil forming processes*, 1994. 147-167, 1994.
- 1000 Pilegaard, K., Skiba, U., Ambus, P., Beier, C., Brüggemann, N., Butterbach-Bahl, K., Dick, J.,
1001 Dorsey, J., Duyzer, J., and Gallagher, M.: Nitrogen load and forest type determine the soil emission
1002 of nitrogen oxides (NO and N₂O), *Biogeosciences Discussions*, 3, 837-869, 2006.
- 1003 Pilegaard, K.: Processes regulating nitric oxide emissions from soils, *Philosophical Transactions*
1004 *of the Royal Society B: Biological Sciences*, 368, 20130126, 2013.
- 1005 Pleim, J.E. and Xiu, A.: Development of a land surface model. Part II: Data assimilation. *Journal*
1006 *of Applied Meteorology*, 42(12), pp.1811-1822, 2003.
- 1007 Pope, C. A., Burnett, R. T., Krewski, D., Jerrett, M., Shi, Y., Calle, E. E., and Thun, M. J.:
1008 Cardiovascular mortality and exposure to airborne fine particulate matter and cigarette smoke:
1009 shape of the exposure-response relationship, *Circulation*, 120, 941-948, 2009.
- 1010 Potter, P., Navin, R., Elena M. B., and Simon D. D.: Characterizing the spatial patterns of global
1011 fertilizer application and manure production. *Earth Interactions*, 14, no. 2: 1-22, 2010.
- 1012 Pouliot, G. and Pierce, T.: Integration of the Model of Emissions of Gases and Aerosols from
1013 Nature (MEGAN) into the CMAQ Modeling System, 2009, 14-17.



- 1014 Pouliot, G.: A tale of two models: a comparison of the Biogenic Emission Inventory System
1015 (BEIS3. 14) and Model of Emissions of Gases and Aerosols from Nature (MEGAN 2.04), 2008.
- 1016 Rasool, Q.Z., R. Zhang, B. Lash, D.S. Cohan, E. Cooter, J. Bash, L.N. Lamsal. Enhanced
1017 representation of soil NO emissions in the Community Multi-scale Air Quality (CMAQ) model
1018 version 5.0.2. *Geoscientific Model Development*, 9, 3177-3197, 2016.
- 1019 Rasool, Q.Z., Bash, J.O., and Cohan, D.S.: Mechanistic representation of soil nitrogen emissions
1020 in CMAQ version 5.1, ORNL DAAC, Oak Ridge, Tennessee, USA,
1021 <https://doi.org/10.3334/ORNLDAAC/1661>, 2018.
- 1022 Redding, M., Shorten, P., Lewis, R., Pratt, C., Paungfoo-Lonhienne, C., and Hill, J.: Soil N
1023 availability, rather than N deposition, controls indirect N₂O emissions, *Soil Biology and*
1024 *Biochemistry*, 95, 288-298, 2016.
- 1025 Ribaudo, M., Key, N., and Sneeringer, S.: The potential role for a nitrogen compliance policy in
1026 mitigating Gulf hypoxia, *Applied Economic Perspectives and Policy*, 39, 458-478, 2016.
- 1027 Robertson, G. P. and Groffman, P.: Nitrogen transformations. In: *Soil Microbiology, Ecology and*
1028 *Biochemistry (Third Edition)*, Elsevier, 2007.
- 1029 Schimel, J. P. and Weintraub, M. N.: The implications of exoenzyme activity on microbial carbon
1030 and nitrogen limitation in soil: a theoretical model, *Soil Biology and Biochemistry*, 35, 549-563,
1031 2003.
- 1032 Schindlbacher, A., Zechmeister-Boltenstern, S., and Butterbach-Bahl, K.: Effects of soil moisture
1033 and temperature on NO, NO₂, and N₂O emissions from European forest soils, *Journal of*
1034 *Geophysical Research: Atmospheres*, 109, 2004.
- 1035 Scholes, M., Martin, R., Scholes, R., Parsons, D., and Winstead, E.: NO and N₂O emissions from
1036 savanna soils following the first simulated rains of the season, *Nutr. Cycl. Agroecosys.*, 48, 115–
1037 122, doi:10.1023/A:1009781420199, 1997.
- 1038 Seinfeld, John H., and Spyros N. Pandis. *Atmospheric chemistry and physics: from air pollution*
1039 *to climate change*. John Wiley & Sons, 2012.



41

- 1040 Simon, H., Reff, A., Wells, B., Xing, J., and Frank, N.: Ozone trends across the United States over
1041 a period of decreasing NO_x and VOC emissions, *Environmental science & technology*, 49, 186-
1042 195, 2014.
- 1043 Skamarock, W. C., Klemp, J. B., Dudhia, J., Gill, D. O., Barker, D. M., Duda, M. G., Huang, X.,
1044 Wang, W., and Powers, J. G.: A description of the advanced research WRF version 3, NCAR Tech.
1045 Note, NCAR/TN-475+STR, 8 pp., Natl. Cent. for Atmos. Res., Boulder, Colo., 2008 (available at:
1046 http://www.mmm.ucar.edu/wrf/users/docs/arw_v3.pdf)
- 1047 Stehfest, E., & Bouwman, L.: N₂O and NO emission from agricultural fields and soils under natural
1048 vegetation: summarizing available measurement data and modeling of global annual emissions.
1049 *Nutrient Cycling in Agroecosystems*, 74(3), 207-228. doi: 10.1007/s10705-006-9000-7, 2006.
- 1050 Steinkamp, J., & Lawrence, M. G.: Improvement and evaluation of simulated global biogenic soil
1051 NO emissions in an AC-GCM. *Atmospheric Chemistry and Physics*, 11(12), 6063–6082.
1052 doi:10.5194/acp-11-6063-2011, 2011.
- 1053 Strode, S. A., Rodriguez, J. M., Logan, J. A., Cooper, O. R., Witte, J. C., Lamsal, L. N., Damon,
1054 M., Van Aartsen, B., Steenrod, S. D., and Strahan, S. E.: Trends and variability in surface ozone
1055 over the United States, *J. Geophys. Res. Atmos.*, 120, 9020–9042, doi:10.1002/2014JD022784,
1056 2015.
- 1057 Su, H., Cheng, Y., Oswald, R., Behrendt, T., Trebs, I., Meixner, F. X., Andreae, M. O., Cheng, P.,
1058 Zhang, Y., and Pöschl, U.: Soil nitrite as a source of atmospheric HONO and OH radicals, *Science*,
1059 333, 1616-1618, 2011.
- 1060 Tilman, D., Fargione, J., Wolff, B., D'antonio, C., Dobson, A., Howarth, R., Schindler, D.,
1061 Schlesinger, W. H., Simberloff, D., and Swackhamer, D.: Forecasting agriculturally driven global
1062 environmental change, *Science*, 292, 281-284, 2001.
- 1063 Townsend, A. R., Howarth, R. W., Bazzaz, F. A., Booth, M. S., Cleveland, C. C., Collinge, S. K.,
1064 Dobson, A. P., Epstein, P. R., Holland, E. A., and Keeney, D. R.: Human health effects of a
1065 changing global nitrogen cycle, *Frontiers in Ecology and the Environment*, 1, 240-246, 2003.
- 1066 Venterea, R. T. and Rolston, D. E.: Mechanisms and kinetics of nitric and nitrous oxide production
1067 during nitrification in agricultural soil, *Global Change Biology*, 6, 303-316, 2000.

41



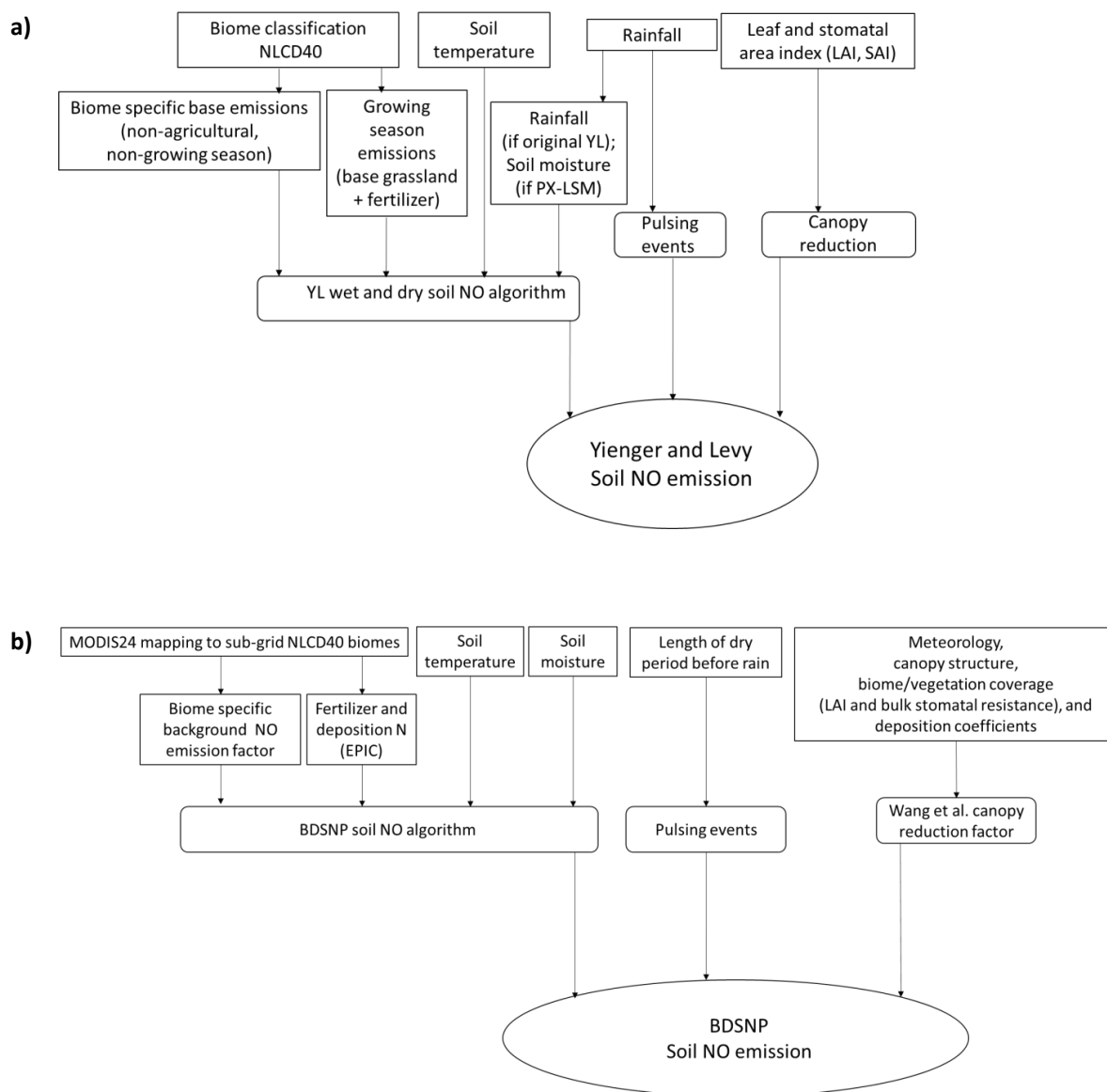
42

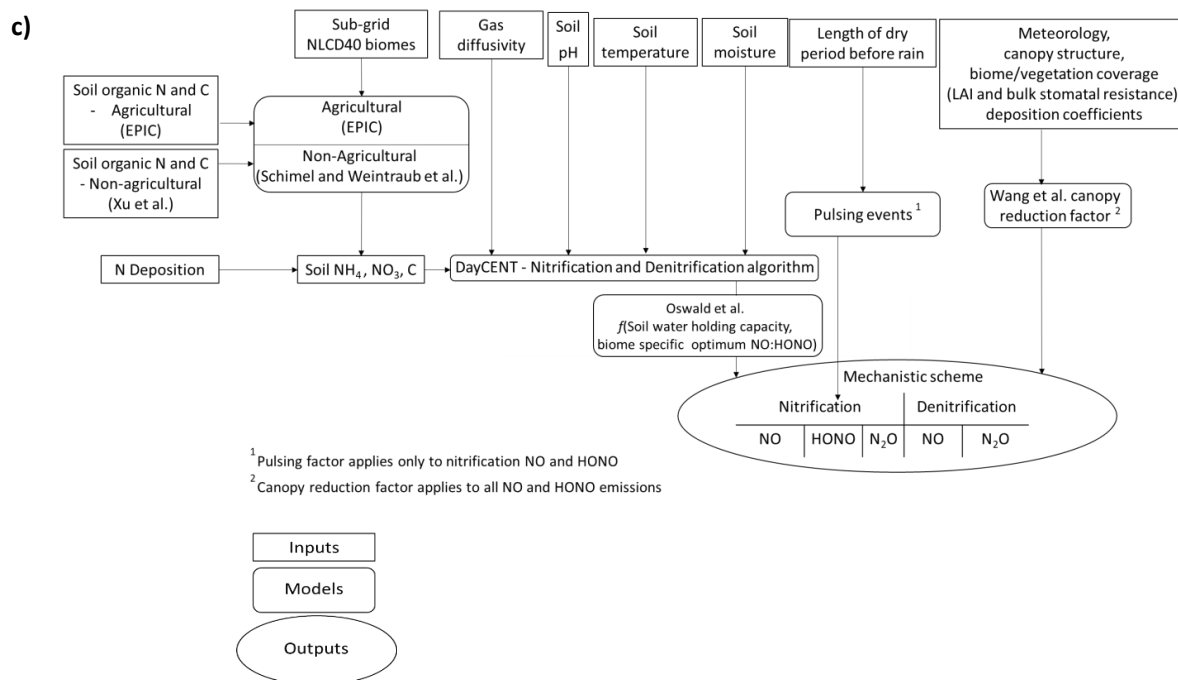
- 1068 Vinken, G. C. M., Boersma, K. F., Maasakkers, J. D., Adon, M., & Martin, R. V. (2014).
1069 Worldwide biogenic soil NO_x emissions inferred from OMI NO₂ observations. *Atmospheric*
1070 *Chemistry and Physics*, 14(18), 10363–10381. doi:10.5194/acp-14-10363-2014.
- 1071 Wade, T., Claassen, R. L., and Wallander, S.: Conservation-practice adoption rates vary widely by
1072 crop and region, United States Department of Agriculture, Economic Research Service, 2015.
- 1073 Wang, C., Houlton, B. Z., Dai, W., and Bai, E.: Growth in the global N₂ sink attributed to N
1074 fertilizer inputs over 1860 to 2000, *Science of the Total Environment*, 574, 1044-1053, 2017.
- 1075 Wang, L., Xu, J., Yang, J., Zhao, X., Wei, W., Cheng, D., Pan, X., and Su, J.: Understanding haze
1076 pollution over the southern Hebei area of China using the CMAQ model, *Atmospheric*
1077 *Environment*, 56, 69-79, 2012.
- 1078 Wang, Y., Logan, J. A., and Jacob, D. J.: Global simulation of tropospheric O₃-NO_x-hydrocarbon
1079 chemistry: 2. Model evaluation and global ozone budget, *Journal of Geophysical Research:*
1080 *Atmospheres* (1984–2012), 103, 10727-10755, 1998.
- 1081 Wang, Y., Zhang, Q. Q., He, K., Zhang, Q., and Chai, L.: Sulfate-nitrate-ammonium aerosols over
1082 China: response to 2000–2015 emission changes of sulfur dioxide, nitrogen oxides, and ammonia,
1083 *Atmos. Chem. Phys.*, 13, 2635-2652, doi:10.5194/acp-13-2635-2013, 2013.
- 1084 Weier, K., Doran, J., Power, J., and Walters, D.: Denitrification and the dinitrogen/nitrous oxide
1085 ratio as affected by soil water, available carbon, and nitrate, *Soil Science Society of America*
1086 *Journal*, 57, 66-72, 1993.
- 1087 Williams, E. and Fehsenfeld, F.: Measurement of soil nitrogen oxide emissions at three North
1088 American ecosystems, *Journal of Geophysical Research: Atmospheres*, 96, 1033-1042, 1991.
- 1089 Williams, E. J., A. Guenther, F. C. Fehsenfeld, An inventory of nitric oxide emissions from soils
1090 in the United States, *J. Geophys. Res.*, 97, 7511–7519, 1992.
- 1091 Williams, E. J., Parrish, D. D., Buhr, M. P., Fehsenfeld, F. C., and Fall, R.: Measurement of soil
1092 NO_x emissions in central Pennsylvania, *J. Geophys. Res.-Atmos.*, 93, 9539–9546,
1093 doi:10.1029/JD093iD08p09539, 1988.

42



- 1094 Williams, J., Izaurralde, R., and Steglich, E.: Agricultural policy/environmental extender model,
1095 Theoretical Documentation, Version, 604, 2008-2017, 2008.
- 1096 Xu, X., Thornton, P. E., and Post, W. M.: A global analysis of soil microbial biomass carbon,
1097 nitrogen and phosphorus in terrestrial ecosystems, *Global Ecology and Biogeography*, 22, 737-
1098 749, 2013.
- 1099 Xu, X., Thornton, P., and POTAPOV, P.: A Compilation of Global Soil Microbial Biomass
1100 Carbon, Nitrogen, and Phosphorus Data, ORNL DAAC, 2015. 2015.
- 1101 Yienger, J. and Levy, H.: Empirical model of global soil-biogenic NO_x emissions, *Journal of*
1102 *Geophysical Research: Atmospheres*, 100, 11447-11464, 1995.
- 1103 Zhu, L., Henze, D., Bash, J., Jeong, G.-R., Cady-Pereira, K., Shephard, M., Luo, M., Paulot, F.,
1104 and Capps, S.: Global evaluation of ammonia bidirectional exchange and livestock diurnal
1105 variation schemes, *Atmos. Chem. Phys.*, 15, 12823–12843, doi:10.5194/acp-15-12823-2015,
1106 2015.
- 1107
- 1108





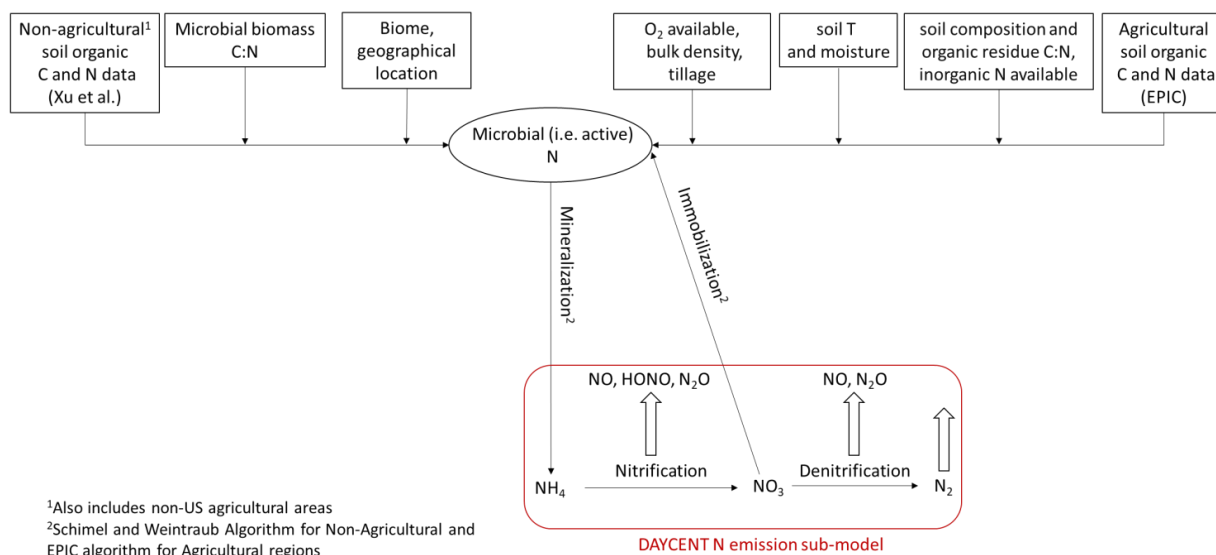
1109 **Figure 1** Flowchart of the a) YL, b) BDSNP, and c) Mechanistic schemes for soil N emissions as
1110 implemented in CMAQ.

1111

1112

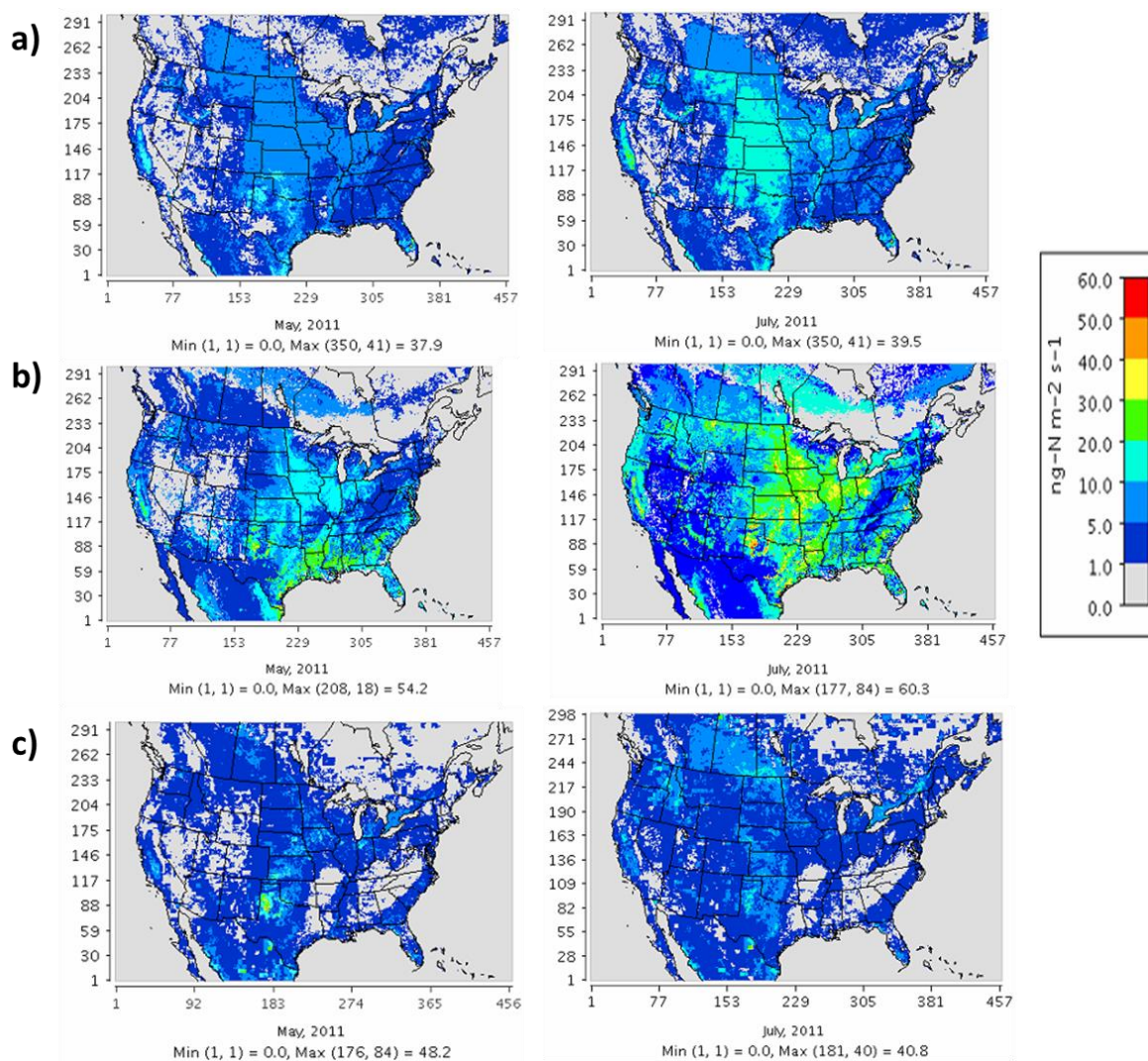
1113

1114



1115

1116 **Figure 2** Schematic for N transformation to estimate soil pools of NH₄ and NO₃ and resultant
 1117 nitrification and denitrification N emissions in the mechanistic model.



1118

1119 **Figure 3** Soil N oxide emissions on a monthly average basis for May (left) and July (right) 2011

1120 for: a) YL scheme (NO), b) Parameterized BDSNP scheme (NO) and c) Mechanistic scheme (NO

1121 + HONO).

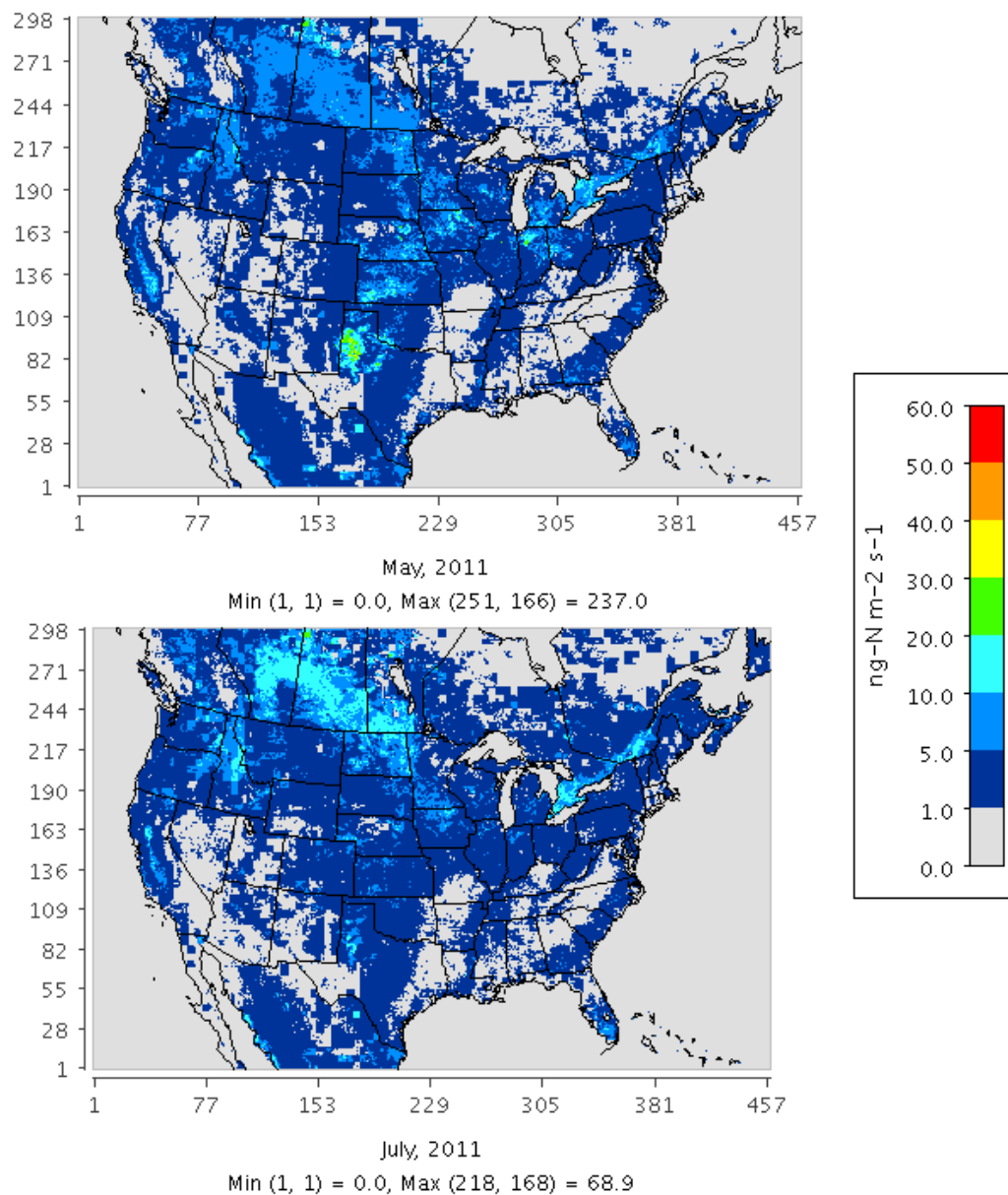
1122

1123

1124

1125

1126



1127

1128 **Figure 4** Soil N₂O emissions on a monthly average basis for May (top) and July (bottom) 2011
1129 estimated from mechanistic scheme.

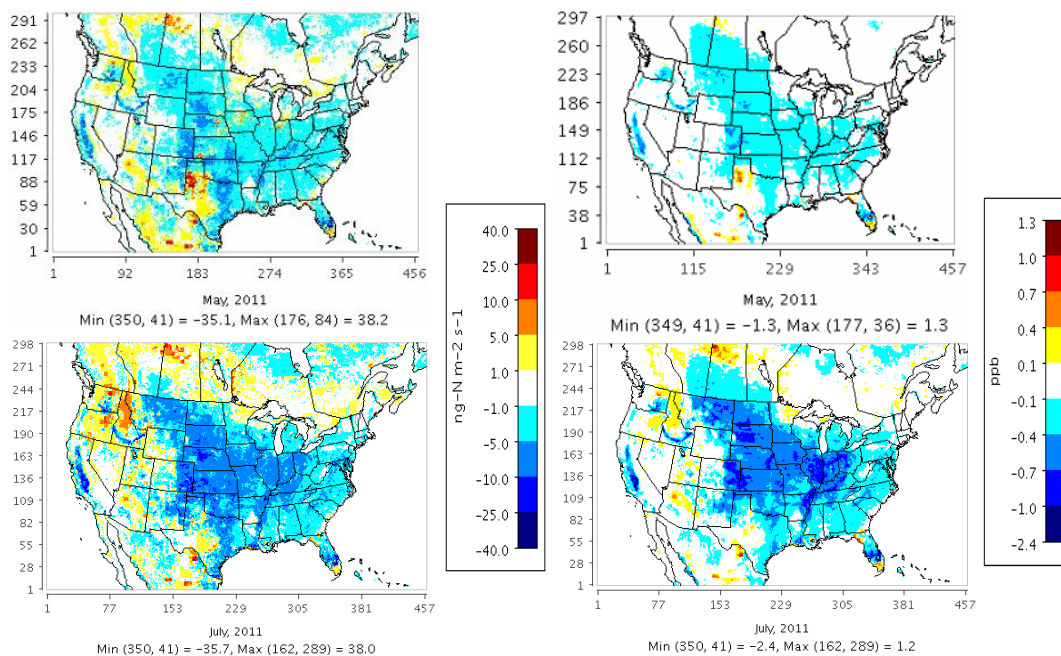
1130

1131

1132



1133



1134

1135 **Figure 5** Total NO_x (NO + NO₂) concentration sensitivity (right) to changes in soil NO_x emissions
1136 (left) on a monthly average basis for May (top) and July (bottom) 2011, when switching from YL
1137 scheme (NO) to Mechanistic scheme (NO + HONO).

1138

1139

1140

1141

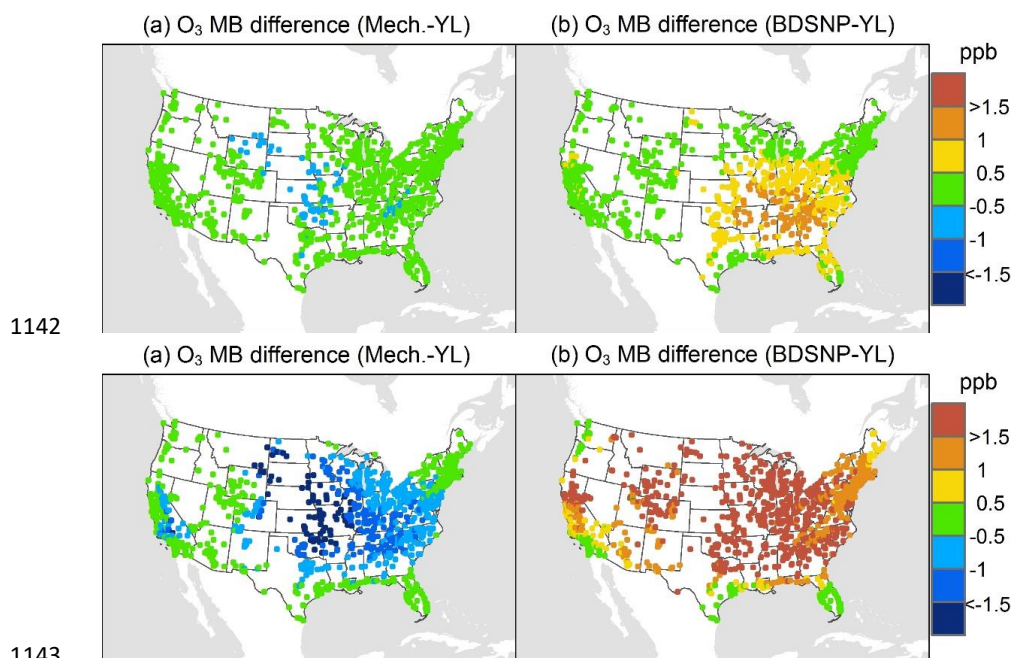


Figure 6 Change in average monthly mean bias (MB) of CMAQ evaluated against AQS O₃ observations for May (top) and July (bottom) 2011 when switching to Mechanistic (a) or BDSNP (b) scheme from YL.

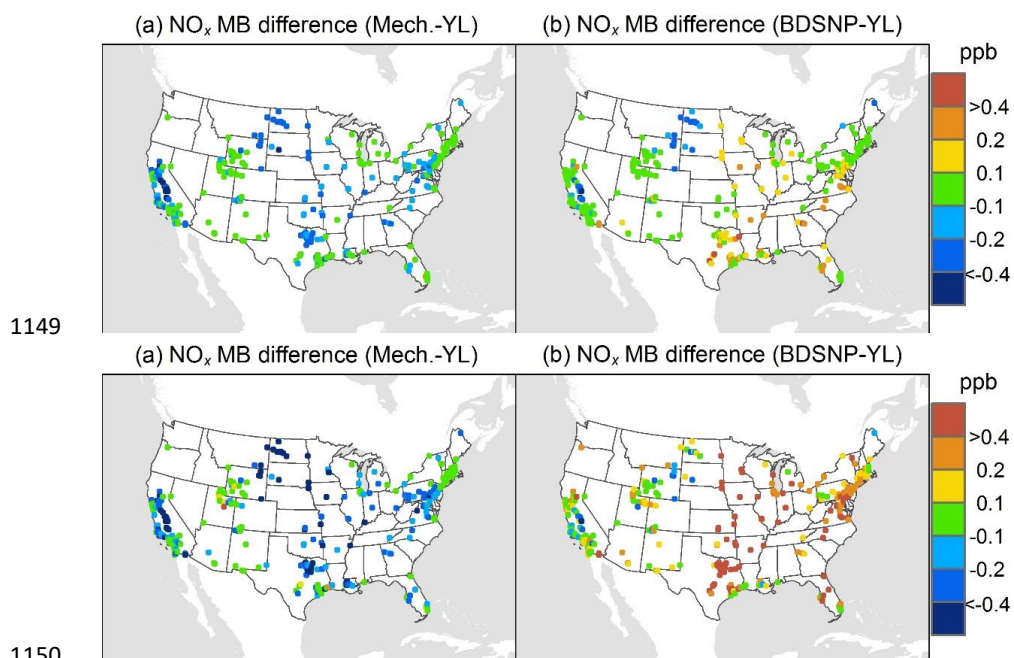
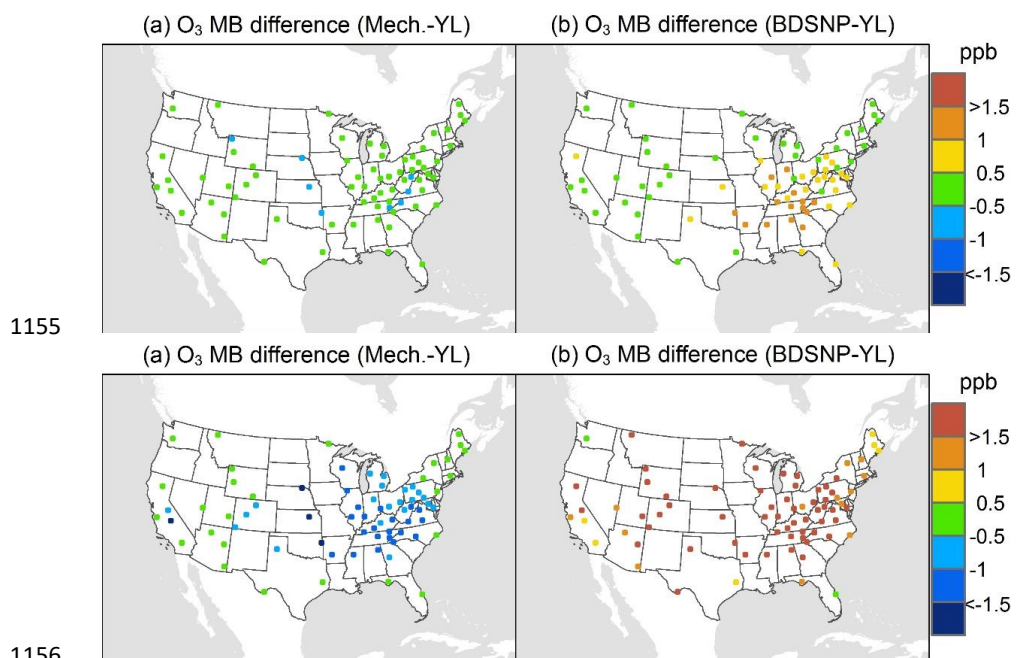


Figure 7 Change in average monthly MB of CMAQ evaluated against AQS NO_x observations for May (top) and July (bottom) 2011 when switching to Mechanistic (a) or BDSNP (b) scheme from YL.



1155

1156

1157

1158 **Figure 8** Change in average monthly MB of CMAQ evaluated against CASTNET O₃ observations
1159 for May (top) and July (bottom) 2011 when switching to Mechanistic (a) or BDSNP (b) scheme
1160 from YL.

1161

1162

1163

1164

1165

1166

1167

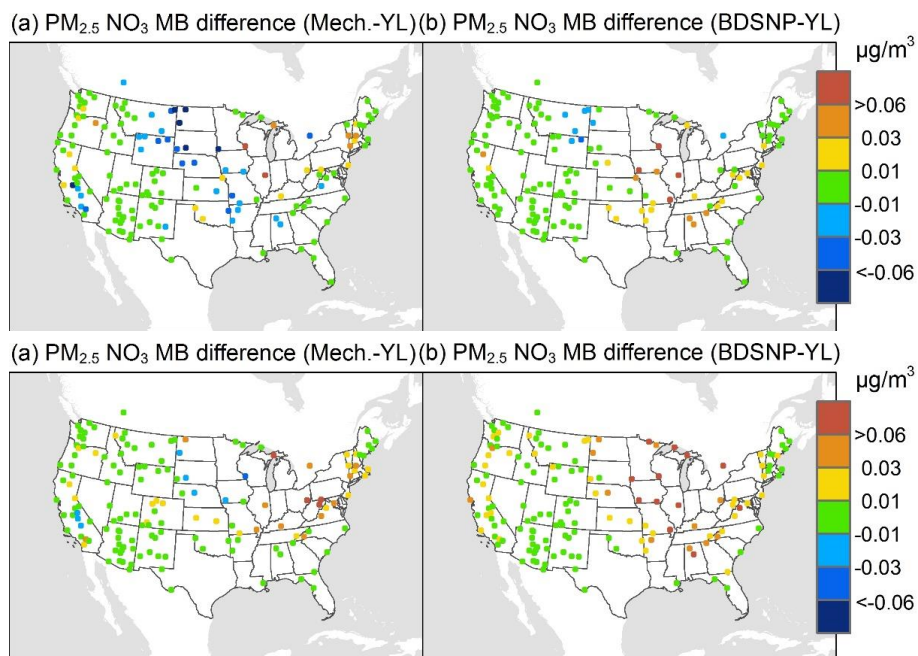


Figure 9 Change in average monthly MB of CMAQ evaluated against IMPROVE $PM_{2.5}$ NO_3 observations for May (top) and July (bottom) 2011 when switching to Mechanistic (a) or BDSNP (b) scheme from YL.

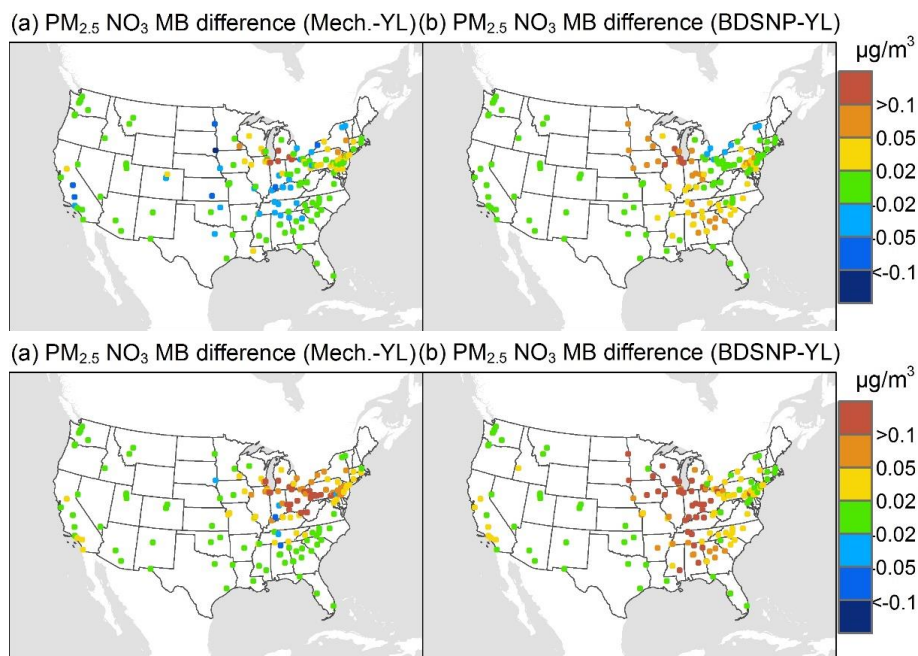
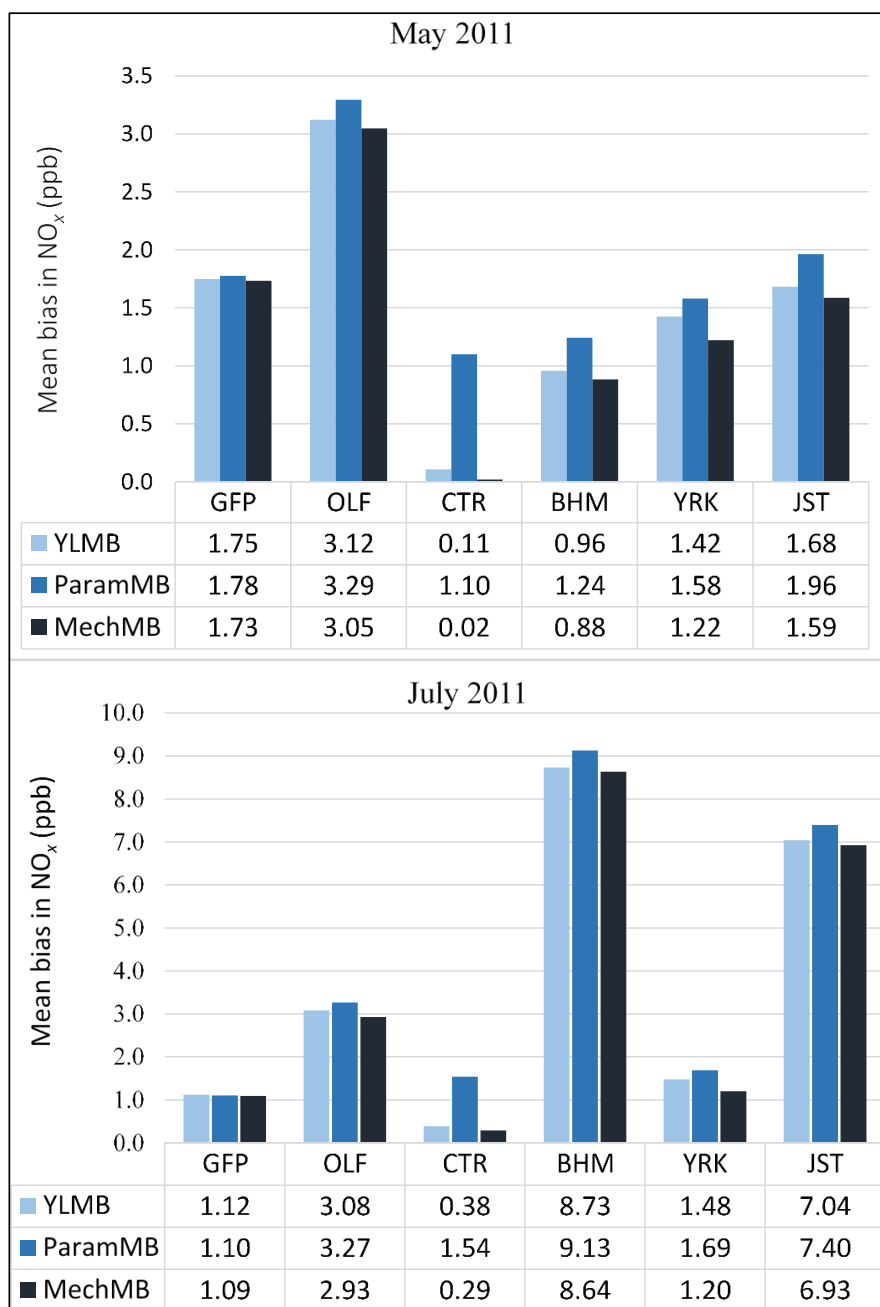


Figure 10 Change in average monthly MB of CMAQ evaluated against CSN PM_{2.5} NO₃ observations for May (top) and July (bottom) 2011 when switching to Mechanistic (a) or BDSNP (b) scheme from YL.



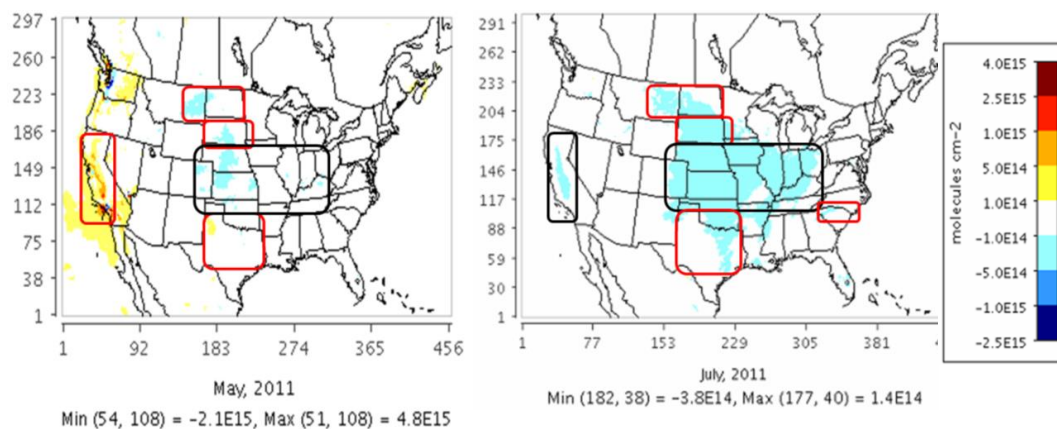
1179

1180

1181

1182

Figure 11 Comparison of average monthly (May and July 2011) MB for CMAQ NO_x with (a) YL
 (b) BDSNP parameterized and (c) Mechanistic schemes compared to SEARCH NO_x observations
 in non-agricultural remote regions.



1183

1184 **Figure 12** Impact of switching from YL scheme to Mechanistic scheme on CMAQ tropospheric
1185 NO₂ column density at OMI overpass time (13:00-14:00 local time) on a monthly average (May
1186 and July 2011) basis.

1187

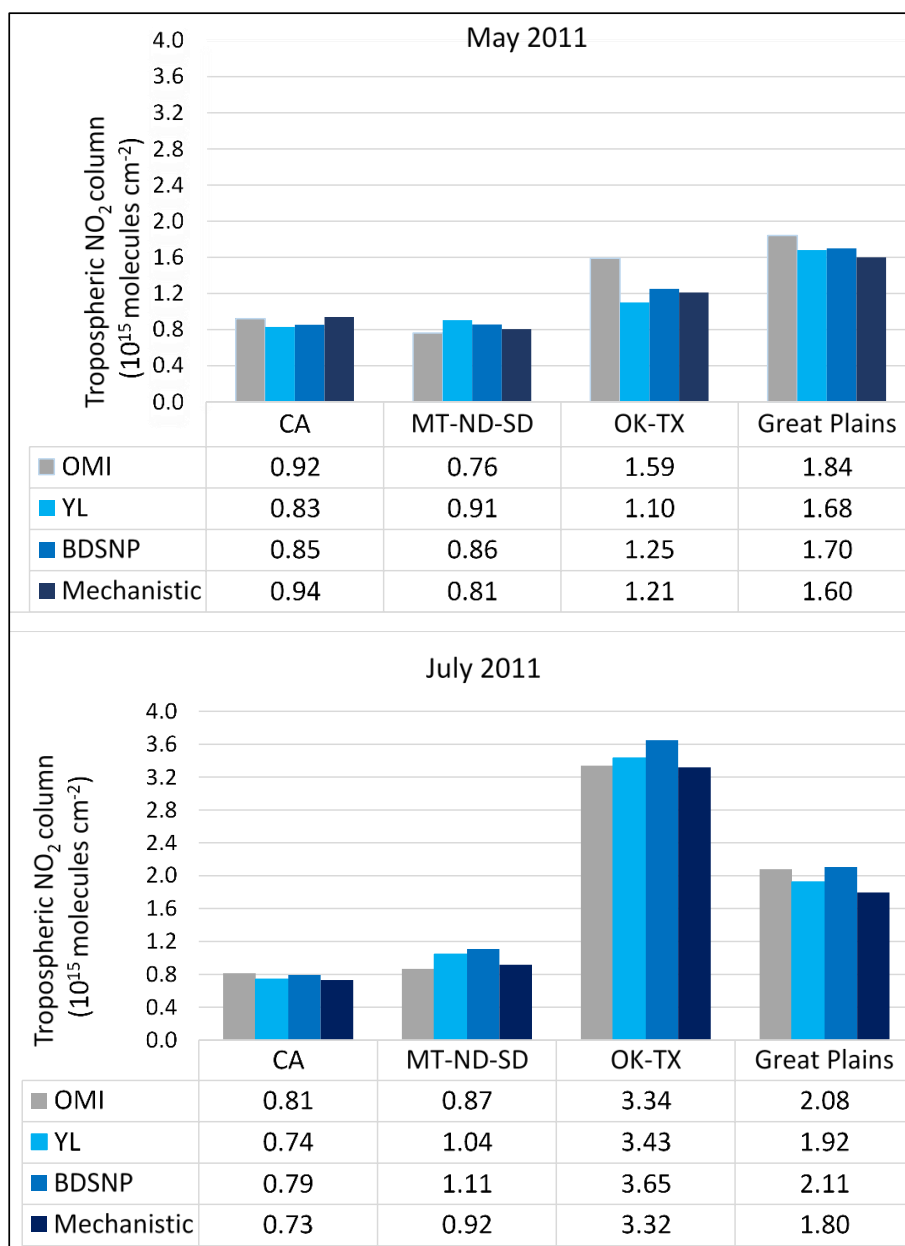
1188

1189

1190

1191

1192



1193

1194

Figure 13 Comparison of average monthly (May and July 2011) OMI NO₂ column densities with

1195

CMAQ tropospheric NO₂ column density using YL, BDSNP, and Mechanistic schemes. Regions

1196

are depicted in Figure 12.

1197

1198



1199 **Table 1:** Comparison of approaches of the parametric and mechanistic soil N emissions models.

	YL Parametric Model	BDSNP Parametric Model	Mechanistic Model
Approach	Yienger and Levy equations for NO	Hudman et al. equations for NO	DayCENT sub-model representing nitrification, denitrification, and mineralization for NO, HONO, and N ₂ O
Species Emitted/Output	NO	NO	NO, HONO, NH ₃ , N ₂ O
Biome/Land use classification	CMAQ default NLCD40	Sub-grid biome classification; MODIS 24 mapped from NLCD40	Sub-grid biome classification from NLCD40
Soil N Data Source	Fertilizer N in growing season wet emission factor	EPIC (Fertilizer N + Deposition (wet and dry) N from CMAQ)	EPIC (Fertilizer N + Deposition (wet and dry) N from CMAQ); Xu et al. (2015) for non-agricultural soil
Agricultural biome	Biome specific NO emission factors	NO emissions derived from total EPIC N	EPIC C and N pools used in DayCENT scheme Nitrification NO, HONO and N ₂ O; Denitrification NO and N ₂ O
Nonagricultural biome	Biome specific NO emission factors	Biome specific NO emission factors	Schimel and Weintraub equations for N and C pools used in DayCENT to derive nitrification and denitrification emissions
Variables Considered	Soil T, rainfall, and biome type	Total soil N, soil T, soil moisture, rainfall, and biome type	Soil water content (irrigated and unirrigated), T, NH ₄ ⁺ , NO ₃ ⁻ , gas diffusivity, and labile C by soil layer
Pulsing	$f(\text{precipitation})$	$f(l_{dry})$, with exponential decay with change in soil moisture	Same as BDSNP
CRF	$f(LAI, SAI)$	$f(LAI, Meteorology, Biome)$	Same as BDSNP

1200

1201

1202

1203



1204 **Table 2** Modeling configuration used for the WRF-CMAQ simulations.

WRF/MCIP			
Version:	ARW V3.7	Shortwave radiation:	RRTMG Scheme
Horizontal resolution:	CONUS (12kmX12km)	Surface layer physic:	PX LSM
Vertical resolution:	35layer	PBL scheme:	ACM2
Boundary condition:	NARR 32km	Microphysics:	Morrison double-moment scheme
Initial condition:	NCEP-ADP	Cumulus parameterization:	Kain-Fritsch scheme
Longwave radiation:	Rapid Radiation Transfer Model Global (RRTMG) Scheme	Assimilation:	Analysis nudging above PBL for temperature, moisture and wind speed
BDSNP			
Horizontal resolution:	Same as WRF/MCIP	Emission factor:	Steinkamp and Lawrence (2011)
Soil Biome type:	Sub-grid biome fractions from WRFv3.7	Fertilizer database:	EPIC 2011 based from FEST-C v1.2
CMAQ			
Version:	5.1	Anthropogenic emission:	NEI 2011 v1
Horizontal resolution:	Same as WRF/MCIP	Biogenic emission:	BEIS v3.61 in-line
Initial condition:	Pleim-Xiu (MET) GEOS-Chem (CHEM)	Boundary condition:	Pleim-Xiu (MET) GEOS-Chem (CHEM)
Aerosol module:	AE6	Gas-phase mechanism:	CB-05
Simulation Case Arrangement (in-line with CMAQ)			
1. YL:	WRF/MCIP-CMAQ with standard YL soil NO scheme		
2. BDSNP (EPIC with new Biome):	WRF/MCIP-BDSNP-CMAQ with EPIC and new sub-grid biome fractions		
3. Mechanistic Scheme:	WRF/MCIP-Mechanistic soil N-CMAQ with EPIC (agricultural US) and Xu et al. (2015) (non-US agricultural and all non-agricultural in CONUS), new sub-grid biome fractions		
Simulation Time Period			
May 1-31 and July 1-31, 2011 (10 day spin-up for each) for CMAQ simulation with in-line YL, updated BDSNP and Mechanistic modules			
Model Performance Evaluation			
USEPA Clean Air Status and Trends Network (CASTNET) and AQS data for ozone			
Interagency Monitoring of Protected Visual Environments (IMPROVE) and Chemical Speciation Network (CSN) (Malm et al., 1994) for PM _{2.5} Nitrate			
AQS and SEARCH for NO _x concentrations			
OMI NO ₂ satellite retrieval product as derived in Lamsal et al., 2014 for NO ₂ column			

1205

1206



1207 **Table 3** NO emission rates ($\text{ng-N m}^{-2} \text{s}^{-1}$) observed in field studies in agricultural and grassland
 1208 locations, and modeled by CMAQ with the three soil N schemes for May and July 2011. Observed
 1209 and modeled values are from peak location/site within a range of values across sites.

Location (Study)	Observed peak summertime soil NO	Mechanistic soil NO ^b		YL soil NO		BDSNP soil NO	
		May 2011	July 2011	May 2011	July 2011	May 2011	July 2011
Iowa fertilized fields (Williams et al., 1992)	18.0	17.1	13.0	8.2	11.4	20.1	41.7
Montana fertilized fields^a (Bertram et al., 2005)	12.0	7.8	14.2	7.1	12.9	9.8	42.3
South Dakota fertilized fields (Williams et al., 1991)	10.0	11.7	10.0	8.0	13.9	18.4	54.6
Texas grasses and fields (both fertilized) (Hutchinson and Brams, 1992)	43.0	52.5	45.0	15.0	15.9	54.1	60.3
Colorado natural grasslands (Parrish et al., 1987; Williams et al., 1991; Martin et al., 1998)	10.0	7.9	11.5	9.7	15.3	18.6	33.2

1210 ^a Derived from SCIAMACHY NO₂ columns

1211 ^b Mechanistic scheme estimates are NO + HONO emission rates

1212

1213

1214



1215 **Table 4** Statistical performance of CMAQ modeled (with YL, updated BDSNP, and Mechanistic
 1216 schemes) tropospheric NO₂ column for May 2011 with OMI NO₂ observations for sensitive sub-
 1217 domains for CONUS.

	Domains	Correlation (r^2)			NMB (%)			NME (%)		
		YL	BDSNP	Mech.	YL	BDSNP	Mech.	YL	BDSNP	Mech.
May	California	0.86	0.86	0.85	-18.6	-17.0	-5.1	35.5	35.4	33.6
	OK-TX	0.19	0.30	0.30	-30.7	-21.7	-23.7	32.2	24.3	25.8
	MT-ND	0.35	0.34	0.34	+24.9	+13.4	+11.1	38.3	35.0	34.3
	SD	0.15	0.16	0.16	+13.4	+11.8	+0.8	27.5	28.6	25.2
	Great Plains	0.68	0.69	0.68	-11.0	-8.7	-14.7	27.8	26.8	29.5
	NC-SC-GA	0.65	0.65	0.65	-4.7	-1.3	-7.0	28.9	27.7	29.9
	CONUS	0.71	0.71	0.70	-10.9	-9.3	-10.6	38.2	37.3	38.6
	California	0.78	0.78	0.79	-17.4	-11.5	-19.0	40.8	41.3	41.8
	OK-TX	0.79	0.79	0.79	+3.0	+9.3	-0.6	17.2	18.0	18.1
	MT-ND	0.44	0.40	0.43	28.5	41.6	13.0	31.6	42.9	23.5
July	SD	0.25	0.16	0.18	15.5	18.8	0.6	20.1	22.8	16.7
	Great Plains	0.69	0.71	0.69	-16.8	-8.6	-22.8	25.4	20.4	30.0
	NC-SC-GA	0.55	0.54	0.55	25.4	31.1	20.9	30.0	33.3	28.8
	CONUS	0.74	0.75	0.72	-12.0	-5.9	-15.0	35.7	34.3	37.4

1218

1219

1220

1221

1222

1223

1224



1225 **Appendix**

1226 **Table A1** List of 24 MODIS soil biome based Cmic, Nmic and HONO_f emission factors (%)

1227 derived from Xu et al. (2013) and Oswald et al. (2013)

ID	MODIS land cover	Köppen main climate ^c	Cmic %	Nmic %	HONO _f %
1	Water	--	0	0	0
2	Permanent wetland	--	1.20	2.58	0
3	Snow and ice	--	0	0	0
4	Barren	D,E	5.02	5.72	48
5	Unclassified	--	0	0	0
6	Barren	A,B,C	5.02	5.72	48
7	Closed shrub land	--	1.43	2.33	35.5
8	Open shrub land	A,B,C	1.43	2.33	41
9	Open shrub land	D,E	1.43	2.33	41
10	Grassland	D,E	2.09	4.28	22
11	Savannah	D,E	1.66	3.61	41
12	Savannah	A,B,C	1.66	3.61	41
13	Grassland	A,B,C	2.09	4.28	22
14	Woody savannah	--	2.09	4.28	41
15	Mixed forest	--	1.29	2.8	13
16	Evergreen broadleaf forest	C,D,E	0.99	2.62	9
17	Deciduous broadleaf forest	C,D,E	1.16	2.42	11
18	Deciduous needle. forest	--	1.79	3.08	8.5
19	Evergreen needle. forest	--	1.76	4.18	8.5
20	Deciduous broadleaf forest	A,B	1.16	2.42	11
21	Evergreen broadleaf forest	A,B	0.99	2.62	9
22	Cropland	--	1.67	2.53	42.9
23	Urban and build-up lands	--	0	0	0
24	Cropland/nat. veg. mosaic	--	1.46	2.62	43.5

1228 ^c A-equatorial, B-arid, C-warm temperature, D-snow, E-polar

1229

1230



1231 **Table A2** Mapping table to create the MODIS 24 soil biome map based on NLCD40 MODIS land
1232 cover categories for updated BDSNP parameterization

NLCD ID	NLCD40 MODIS CATEGORY (40)	MODIS ID	SOIL BIOME CATEGORY (24)
1	Evergreen Needle leaf Forest	19	Evergreen Needle leaf Forest
2	Evergreen Broadleaf Forest	16 and 21	Evergreen Broadleaf Forest
3	Deciduous Needle leaf Forest	18	Dec. Needle leaf Forest
4	Deciduous Broadleaf Forest	17 and 20	Dec. Broadleaf Forest
5	Mixed Forests	15	Mixed Forest
6	Closed shrublands	7	Closed shrublands
7	Open shrublands	8 and 9	Open shrublands
8	Woody Savannas	14	Woody savannah
9	Savannas	11 and 12	Savannah
10	Grasslands	10 and 13	Grassland
11	Permanent Wetlands	2	Permanent Wetland
12	Croplands	22	Cropland
13	Urban and Built Up	23	Urban and build-up lands
14	Cropland-Natural Vegetation Mosaic	24	Cropland/nat. veg. mosaic
15	Permanent Snow and Ice	3	Snow and ice
16	Barren or Sparsely Vegetated	6	Barren
17	IGBP Water	1	Water
18	Unclassified	4	Barren ^d
19	Fill value	5	Unclassified ^d
20	Open Water	1	Water
21	Perennial Ice-Snow	3	Snow and ice
22	Developed Open Space	23	Urban and build-up lands
23	Developed Low Intensity	23	Urban and build-up lands
24	Developed Medium Intensity	23	Urban and build-up lands
25	Developed High Intensity	23	Urban and build-up lands
26	Barren Land (Rock-Sand-Clay)	24	Cropland/nat. veg. mosaic
27	Unconsolidated Shore	24	Cropland/nat. veg. mosaic
28	Deciduous Forest	16 and 21	Evergreen Broadleaf Forest
29	Evergreen Forest	19	Evergreen Needle leaf Forest
30	Mixed Forest	15	Mixed Forest
31	Dwarf Scrub	8 and 9	Open shrublands
32	Shrub-Scrub	8 and 9	Open shrublands
33	Grassland-Herbaceous	10 and 13	Grassland
34	Sedge-Herbaceous	14	Woody savannah
35	Lichens	10 and 13	Grassland
36	Moss	10 and 13	Grassland
37	Pasture-Hay	24	Cropland/nat. veg. mosaic
38	Cultivated Crops	22	Cropland
39	Woody Wetlands	2	Permanent Wetland
40	Emergent Herbaceous Wetlands	2	Permanent Wetland

1233 ^d NLCD categories 18 and 19 were mapped as MODIS category 1 (Water) in Rasool et al. (2016), which have been
1234 corrected here.



1235 **Table A3** Microbial/Organic biomass C and N % and HONO/N_{NOx} % mapped to respective
 1236 NLCD40 MODIS land-cover categories based on Xu et al. (2013) estimates

NLCD ID	NLCD40 MODIS CATEGORY (40)	Cmic %	Nmic %	HONO _f %
1	Evergreen Needle leaf Forest	1.76	4.18	8.5
2	Evergreen Broadleaf Forest	0.99	2.62	9
3	Deciduous Needle leaf Forest	1.79	3.08	8.5
4	Deciduous Broadleaf Forest	1.16	2.42	11
5	Mixed Forests	1.29	2.80	13
6	Closed shrublands	1.43	2.33	35.5
7	Open shrublands	1.43	2.33	41
8	Woody Savannas	2.09	4.28	41
9	Savannas	1.66	3.61	41
10	Grasslands	2.09	4.28	22
11	Permanent Wetlands	1.2	2.58	0
12	Croplands	1.67	2.53	42.9
13	Urban and Built Up	0	0	0
14	Cropland-Natural Vegetation Mosaic	1.46	2.62	43.5
15	Permanent Snow and Ice	0	0	0
16	Barren or Sparsely Vegetated	5.02	5.72	48
17	IGBP Water	0	0	0
18	Unclassified	5.02	5.72	48
19	Fill value	0	0	0
20	Open Water	0	0	0
21	Perennial Ice-Snow	0	0	0
22	Developed Open Space	0	0	0
23	Developed Low Intensity	0	0	0
24	Developed Medium Intensity	0	0	0
25	Developed High Intensity	0	0	0
26	Barren Land (Rock-Sand-Clay) ^e	0	0	0
27	Unconsolidated Shore ^e	0	0	0
28	Deciduous Forest	0.99	2.62	9
29	Evergreen Forest	1.76	4.18	8.5
30	Mixed Forest	1.29	2.8	13
31	Dwarf Scrub	1.43	2.33	41
32	Shrub-Scrub	1.43	2.33	41
33	Grassland-Herbaceous	2.09	4.28	22
34	Sedge-Herbaceous	2.09	4.28	41
35	Lichens	2.09	4.28	22
36	Moss	2.09	4.28	22
37	Pasture-Hay ^f	0	0	43.5
38	Cultivated Crops ^f	0	0	42.9
39	Woody Wetlands	1.2	2.58	0
40	Emergent Herbaceous Wetlands	1.2	2.58	0

1237 ^e NLCD classes 26 and 27 constituting of rocks mostly. ^f Cmic and Nmic for US croplands classified under NLCD classes
 1238 37 and 38 are kept as zero to prevent double counting, as they are accounted for by EPIC N data.